Appendix A
Definitions and Conventions Used Throughout the Work

This appendix contains the definitions and conventions which are used throughout the work. They are ordered in the way they are used in the text. In some cases, more than one, slightly different, definition is available for the same subject. In this case a choice is made and if needed, it will be argued why this particular definition is chosen.

A.1 The Fourier Transform and Fourier Series

A signal can be represented in the time domain as well as in the frequency domain. A difference is made between non-periodic and periodic waveforms.

A.1.1 Non-periodic Waveforms

To obtain the frequency spectrum of a signal, the Fourier transform is used [34]:

Definition A.1 The Fourier transform of a waveform $w(t)$ is:

$$W(f) = \mathscr{F}[w(t)] = \int_{-\infty}^{\infty} w(t) \cdot e^{-j \cdot 2 \cdot \pi \cdot f \cdot t} dt \tag{A.1}$$

where $\mathscr{F}[w(t)]$ denotes the Fourier transform of $w(t)$ and f is the frequency parameter with units of Hz. This *defines* the term frequency, which is the parameter f in the Fourier transform.

V. De Smedt et al., *Temperature- and Supply Voltage-Independent Time References for Wireless Sensor Networks*, Analog Circuits and Signal Processing 128,
DOI 10.1007/978-3-319-09003-0

Note that instead of the frequency, also the angular frequency $\omega = 2 \cdot \pi \cdot f$ can be used in the Fourier transform. Although this sometimes simplifies the mathematics, it is less intuitive when measuring for instance a spectrum with a spectrum analyzer. The Fourier transform results in a *two-sided* spectrum since both positive and negative frequencies are obtained from the definition. Often the Fourier transform of a waveform is split in a magnitude and a phase function:

$$W(f) = |W(f)| \cdot e^{j \cdot \theta(f)} \tag{A.2}$$

$$\text{in which: } |W(f)| = \sqrt{\Im[W(f)]^2 + \Re[W(f)]^2} \tag{A.3}$$

$$\text{and: } \theta(f) = \arctan\left(\frac{\Im[W(f)]}{\Re[W(f)]}\right) \tag{A.4}$$

which is called the *polar form* of the Fourier transform. The inverse Fourier transform can be used to, starting from a complex frequency spectrum, obtain the original waveform:

Definition A.2 The inverse Fourier transform of a frequency spectrum $F(f)$ is:

$$w(t) = \mathscr{F}^{-1}[W(f)] = \int_{-\infty}^{\infty} W(f) \cdot e^{j \cdot 2 \cdot \pi \cdot f \cdot t} df \tag{A.5}$$

where $\mathscr{F}^{-1}[W(f)]$ denotes the Inverse Fourier transform of $W(f)$.

$w(t)$ and $W(f)$ are called Fourier pairs. The existence of the Fourier transform of a waveform is, however, not always guaranteed since the infinite integral can diverge. Different conditions can be used to check whether the Fourier transform exists for a waveform $w(t)$. These conditions are all *sufficient*, but *not necessary* [34]:

- $w(t)$ is absolutely integrable:

$$\int_{-\infty}^{\infty} |w(t)| dt < \infty \tag{A.6}$$

  and, over any time interval of finite width, the function $w(t)$ is a single-valued function with a finite number of maxima and minima, and the number of discontinuities (if any) is finite.
- The normalized energy (2-norm) of the waveform is finite:

$$E = \int_{-\infty}^{\infty} |w(t)|^2 dt < \infty \tag{A.7}$$

The first conditions are called the *Dirichlet conditions*, the second is the finite-energy condition which is somewhat weaker and satisfied for every physical waveform!

A.1.1.1 Properties of the Fourier transform

When doing calculations with waveforms or when calculating the spectrum of a waveform, different properties can be useful. Some of them are briefly summarized in this section, a more complete overview can be found in [34].

- The spectrum of a real waveform is symmetrical:

$$W(-f) = \overline{W(f)} \tag{A.8}$$

  in which $\overline{W(f)}$ is the complex conjugate. When using the polar notation, this means:

$$W(-f) = |W(f)| \cdot e^{-j\cdot\theta(f)} \tag{A.9}$$

- The frequency f is just a parameter of the Fourier transform that specifies the frequency of interest. The Fourier transform looks for this frequency over all time $-\infty < t < \infty$.
- $W(f)$ can be complex, also for real waveforms $w(t)$.
- Linearity: $\mathcal{F}[a_1 \cdot f(t) + a_2 \cdot g(t)] = a_1 \cdot F(f) + a_2 \cdot G(f)$
- Time delay: $\mathcal{F}[w(t-\tau)] = W(f) \cdot e^{-j\cdot\omega\cdot\tau}$
- Complex signal frequency translation: $\mathcal{F}[w(t) \cdot e^{j\cdot\omega_c\cdot t}] = W(f - f_c)$
- Differentiation:

$$\mathcal{F}\left[\frac{d^n w(t)}{dt^n}\right] = (j \cdot 2 \cdot \pi \cdot f)^n \cdot W(f) \tag{A.10}$$

- Integration:

$$\mathcal{F}\left[\int_{-\infty}^{t} w(t)\right] = (j \cdot 2 \cdot \pi \cdot f)^{-1} \cdot W(f) + \frac{1}{2} \cdot W(0) \cdot \delta(f) \tag{A.11}$$

- Convolution:

$$\mathcal{F}\left[f(t) * g(t)\right] = F(f) \cdot G(f) \tag{A.12}$$

- Multiplication:

$$\mathcal{F}\left[f(t) \cdot g(t)\right] = F(f) * G(f) \tag{A.13}$$

Extra attention is needed for a commonly used property of a signal and its Fourier transform, called *Parseval's theorem*:

Theorem A.1 *For two signals $f(t)$ and $g(t)$, with Fourier transforms $F(f)$ and $G(f)$:*

$$\int_{-\infty}^{\infty} f(t) \cdot \overline{g(t)} dt = \int_{-\infty}^{\infty} F(f) \cdot \overline{G(f)} df \tag{A.14}$$

where $\overline{g(t)}$ denotes the complex conjugate of $g(t)$. When $f(t) = g(t)$, this reduces to:

$$\int_{-\infty}^{\infty} |f(t)|^2 dt = \int_{-\infty}^{\infty} |F(f)|^2 df \tag{A.15}$$

which is known as Rayleigh's energy theorem.

A.1.2 Periodic Waveforms

It can be shown that a waveform $w(t)$ can be represented by a sum of orthogonal functions $\varphi_n(t)$ in the interval (a, b) using the following theorem [34]:

Theorem A.2 *$w(t)$ can be represented over the interval (a, b) by the series*

$$w(t) = \sum_n a_n \cdot \varphi_n(t) \tag{A.16}$$

where the orthogonal coefficients are given by

$$a_n = \frac{1}{K_n} \cdot \int_a^b w(t) \cdot \overline{\varphi_n(t)} dt \tag{A.17}$$

$$and{:}K_n = \int_a^b \varphi_n(t) \cdot \overline{\varphi_n(t)} dt \tag{A.18}$$

and the range of n is over the integer values that correspond to the subscripts that where used to denote the orthogonal functions in the complete orthogonal set.

A complete set $\{\varphi_n(t)\}$ of orthogonal functions means that any function can be represented with an arbitrarily small error using the functions in $\{\varphi_n(t)\}$. This is, however, difficult to prove. A set of complex exponential functions and a set of harmonic sinusoids can, however, be proven to be complete [36]. These sets are used to define the Fourier series.

Theorem A.3 *A physical waveform can be represented over the interval $a < t < a + T_0$ by the complex exponential Fourier series*

$$w(t) = \sum_{n=-\infty}^{n=\infty} c_n \cdot e^{j \cdot n \cdot \omega_0 \cdot t} \tag{A.19}$$

where the complex Fourier coefficients are:

$$c_n = \frac{1}{T_0} \cdot \int_a^{a+T_0} w(t) \cdot e^{-j \cdot n \cdot \omega_0 \cdot t} dt \tag{A.20}$$

and where $\omega_0 = 2 \cdot \pi \cdot f_0 = 2 \cdot \pi / T_0$.

For waveforms which are periodic with period T_0, this Fourier series is a representation of the function over all time because all functions of the orthogonal set are periodic with the same fundamental period as $w(t)$, T_0. The Fourier series can therefore be seen as a special case of the Fourier transform for periodic functions. The spectrum in this case consists of discrete lines at the harmonic frequencies. Also the properties of the Fourier transform can be used for the Fourier series:

- If $w(t)$ is real, $c_n = \overline{c_{-n}}$
- If $w(t)$ is real and $w(t) = w(-t)$, $\Im[c_n] = 0$
- If $w(t)$ is real and $w(t) = -w(-t)$, $\Re[c_n] = 0$
- Parseval's theorem is:

$$\frac{1}{T_0} \cdot \int_a^{a+T_0} |w(t)|^2 dt = \sum_{n=-\infty}^{n=\infty} |c_n|^2 \tag{A.21}$$

In some applications it can be useful to use the *quadrature* form of the Fourier series:

Theorem A.4 *A physical waveform $w(t)$ can be represented over the interval $a < t < a + T_0$ by a sum of sinusoids:*

$$w(t) = \sum_{n=0}^{n=\infty} a_n \cdot \cos(n \cdot \omega_0 \cdot t) + \sum_{n=1}^{n=\infty} b_n \cdot \sin(n \cdot \omega_0 \cdot t) \tag{A.22}$$

where the orthogonal functions are $\sin(n \cdot \omega_0 \cdot t)$ *and* $\cos(n \cdot \omega_0 \cdot t)$*, and the coefficients are given by:*

$$a_n = \begin{cases} \frac{1}{T_0} \cdot \int_a^{a+T_0} w(t) dt & \text{for } n = 0 \\ \frac{2}{T_0} \cdot \int_a^{a+T_0} w(t) \cdot \cos(n \cdot \omega_0 \cdot t) dt & \text{for } n \geq 1 \end{cases} \tag{A.23}$$

and:

$$b_n = \frac{2}{T_0} \cdot \int_a^{a+T_0} w(t) \cdot \sin(n \cdot \omega_0 \cdot t) dt \quad \text{for } n \geq 1 \tag{A.24}$$

The relation between the coefficients of the complex and the quadrature Fourier series is:

$$a_n = \begin{cases} c_0 & \text{for } n = 0 \\ 2 \cdot \Re(c_n) & \text{for } n \geq 1 \end{cases} \tag{A.25}$$

and,

$$b_n = -2 \cdot \Im(c_n) \quad \text{for } n \geq 1 \tag{A.26}$$

A last form of the Fourier series is the polar form:

Theorem A.5 *A physical waveform $w(t)$ can be represented over the interval $a < t < a + T_0$ by a sum of sinusoids:*

$$w(t) = D_0 + \sum_{n=1}^{n=\infty} D_n \cdot \cos(n \cdot \omega_0 \cdot t + \varphi_n) \tag{A.27}$$

where $w(t)$ is real and:

$$D_n = \begin{cases} a_0 = c_0 & \textit{for } n = 0 \\ \sqrt{a_n^2 + b_n^2} = 2 \cdot |c_n| & \textit{for } n \geq 1 \end{cases} \tag{A.28}$$

and:

$$\varphi_n = -arctan\left(\frac{b_n}{a_n}\right) = \angle c_n \quad \textit{for } n \geq 1 \tag{A.29}$$

In this work, both the complex and the quadrature form of the Fourier series are used, depending on the situation. It is clear that both forms have their benefits: the ease of mathematical calculations for the complex waveform and the intuitive approach of the quadrature and polar form.

A.2 The Autocorrelation and PSD of a Signal

The autocorrelation and the Power Spectral Density (PSD) of a time signal contain the same information about a signal since the PSD of a random signal is defined as the Fourier transform of its autocorrelation function [41]. Before formulating the formulas of the autocorrelation and the PSD, the definitions of a stationary signal and an ergodic signal are needed:

Definition A.3 A random process $x(t)$ is said to be stationary to the order N if, for any $t_1, t_2, ..., t_N$:

$$f_x(x(t_1), x(t_2), ..., x(t_N)) = f_x(x(t_1 + t_0), x(t_2 + t_0), ..., x(t_N + t_0)) \tag{A.30}$$

where t_0 is an arbitrary real constant and $f_x(\mathbf{x})$ is an N-dimensional Probability Density Function (PDF). The process is said to be strictly stationary if it is stationary to the order $N \to \infty$.

The first-order stationarity of a random process can thus easily be checked by determining whether its first-order PDF is a function of time.

Definition A.4 A random process is said to be ergodic if all time averages of any sample function are equal to the corresponding ensemble averages (expectations).

Since ergodicity is not the most straightforward concept to understand, an example is given to illustrate this:

Example A.1 In electrical engineering, two commonly used averages are the **dc** and **rms** values. These values are both defined (and measured) as time averages. However, when the process is ergodic, also ensemble averages can be used.

- The dc value of a random process $x(t)$ is by definition equal to:

$$x_{dc} \triangleq \lim_{T\to\infty} \frac{1}{T} \cdot \int_{-T/2}^{T/2} [x(t)]dt \tag{A.31}$$

  which is, in the case of an ergodic process, equivalent to:

$$E[x(t)] = \int_{-\infty}^{\infty} [x \cdot f_x(x)]dx = m_x \tag{A.32}$$

  where $E[x(t)]$ or m_x is the expected or mean value of $x(t)$.
- The rms value of a random process $x(t)$ is by definition equal to:

$$x_{rms} \triangleq \sqrt{\lim_{T\to\infty} \frac{1}{T} \cdot \int_{-T/2}^{T/2} [x(t)^2]dt} \tag{A.33}$$

  which is, in the case of an ergodic process, equivalent to:

$$\sqrt{E[x(t)^2]} = \sqrt{\sigma_x^2 + m_x^2} \tag{A.34}$$

where $E[x(t)^2]$ is the expected or mean value of $x(t)^2$ and σ_x^2 is the variance of $x(t)$.

A.2.1 The Autocorrelation

The autocorrelation of a signal is defined as the correlation between the signal and a time-shifted version of itself.

Definition A.5 The autocorrelation of a quadratically infinitely integrable signal $f(t)$ is most often defined as the continuous cross-correlation of the signal with itself:

$$R_f(\tau) = \int_{-\infty}^{\infty} f(t) \cdot \overline{f(t-\tau)} dt \tag{A.35}$$

$$= \int_{-\infty}^{\infty} f(t+\tau/2) \cdot \overline{f(t-\tau/2)} dt \tag{A.36}$$

$$= \int_{-\infty}^{\infty} f(t+\tau) \cdot \overline{f(t)} dt \tag{A.37}$$

where $\overline{f(t)}$ is the complex conjugate of $f(t)$. For real signals this complex conjugate can be omitted.

For signals which last forever and are therefore often not quadratically infinitely integrable, an alternative definition of the autocorrelation is used:

Definition A.6

$$R_f(\tau) = \lim_{T\to\infty} \frac{1}{T} \cdot \int_{-T/2}^{T/2} \overline{f(t)} \cdot f(\tau - t) dt \tag{A.38}$$

when $f(t)$ is ergodic or stationary in the wide sense.

In this thesis, since most of the discussed signals are oscillator outputs which can last forever, definition (A.6) is used.

A.2.2 The Power Spectral Density

The power spectral density of a signal is a representation of the power in a signal in the frequency domain. It can be defined as the Fourier transform of the autocorrelation function of the signal (the *Wiener-Khinchine* theorem) [34]:

Definition A.7 The Power Spectral Density of a signal $f(t)$ with autocorrelation function $R_f(\tau)$ is calculated as the Fourier transform of $R_f(\tau)$:

$$S_f(\omega) = \int_{-\infty}^{\infty} R_f(\tau) \cdot e^{-j \cdot \omega \cdot \tau} d\tau \tag{A.39}$$

It follows that the autocorrelation of a signal $f(t)$ with PSD $S_f(\omega)$ can be calculated as:

$$R_f(\omega) = \frac{1}{2 \cdot \pi} \cdot \int_{-\infty}^{\infty} R_f(\tau) \cdot e^{j \cdot \omega \cdot \tau} d\tau \tag{A.40}$$

The power of a signal in a certain frequency band $[\omega_1, \omega_2]$ can then be calculated by integrating over positive as well as negative frequencies:

$$P_{\omega_1,\omega_2} = \int_{\omega_1}^{\omega_2} (S_f(\omega) + S_f(-\omega)) d\omega \tag{A.41}$$

For real signals, the PSD is symmetrical around zero. Alternatively, the power spectral density can be defined as follows:

Definition A.8 The average power in a signal $f(t)$ is defined as:

$$\mathscr{P}\{f(t)\} = \lim_{T \to \infty} \frac{1}{T} \cdot \int_{-T/2}^{T/2} |f(t)|^2 dt \tag{A.42}$$

Let:

$$f_T(t) = f(t) \cdot \Pi\left(\frac{t}{T}\right) \tag{A.43}$$

and using Parseval's theorem, this can be written as:

$$\mathscr{P}\{f(t)\} = \lim_{T\to\infty} \frac{1}{T} \cdot \int_{-\infty}^{\infty} |F_T(f)|^2 df \tag{A.44}$$

$$= \int_{-\infty}^{\infty} S_f(f) df \tag{A.45}$$

where

$$S_f(f) = \lim_{T\to\infty} \frac{1}{T} \cdot |F_T(f)|^2 \tag{A.46}$$

is called the *Power Spectral Density*.

It must be noted that both definitions lead to exactly the same result. The first calculation method is often called the *indirect* calculation method; the second, *direct*, calculation method has no need for calculating the autocorrelation first. The unit of the PSD is *watt per hertz*, W/Hz. For practical reasons mostly the single-sided PSD is used, as will be indicated throughout the work.

A.3 Generalized and Special Functions

In this section some of the commonly used functions are defined in order to avoid any confusion with other definitions which are sometimes used. The definitions used are the same as in [34].

A.3.1 The Dirac Delta Function

Definition A.9 The Dirac delta function $\delta(x)$ is defined by:

$$\int_{-\infty}^{\infty} w(x) \cdot \delta(x) = w(0) \tag{A.47}$$

where $w(x)$ is a continuous function at $x = 0$.

Depending on the application x can be time or frequency or some other variable. An alternative definition of $\delta(x)$ is:

Definition A.10 The Dirac delta function $\delta(x)$ is defined by:

$$\int_{-\infty}^{\infty} \delta(x) = 1 \tag{A.48}$$

and:

$$\delta(x) = \begin{cases} \infty & \text{for } x = 0 \\ 0 & \text{for } x \neq 0 \end{cases} \tag{A.49}$$

Since the Dirac function is not a real function (it contains singularities), it is called a singular function. In some situations, it can be useful to use the equivalent integral of the δ function:

$$\delta(x) = \int_{-\infty}^{\infty} e^{\pm j \cdot 2 \cdot \omega \cdot x \cdot y} dy \tag{A.50}$$

This can be proven by noting that the Fourier transform of the delta function is equal to 1. By calculating the inverse Fourier transform, the equivalent integral is obtained.

A.3.2 The Step Function

The step or Heaviside function is often used when calculating Laplace transforms.

Definition A.11 The unit step function $u(t)$ is

$$u(t) = \begin{cases} 1 & \text{for } t > 0 \\ 0 & \text{for } t < 0 \end{cases} \tag{A.51}$$

The relation between the unit step function and the Dirac function is:

$$\int_{-\infty}^{t} \delta(x)dx = u(t) \tag{A.52}$$

$$\frac{du(t)}{t} = \delta(t) \tag{A.53}$$

The Fourier transform of the unit step function is equal to:

$$\mathscr{F}[u(t)] = \frac{1}{2} \cdot \delta(f) + \frac{1}{j \cdot 2 \cdot \pi \cdot f} \tag{A.54}$$

A.3.3 A Rectangular Pulse

A rectangular pulse is often used to consider a function only over a certain interval.

Definition A.12 Let $\Pi[\cdot]$ denote a single rectangular pulse with duration T, then:

$$\Pi\left[\frac{t}{T}\right] \triangleq \begin{cases} 1, & |t| \leq \frac{T}{2} \\ 0, & |t| > \frac{T}{2} \end{cases} \tag{A.55}$$

The Fourier transform of this function is equal to the *sinc* function:

$$\text{sinc}(x) = \frac{\sin(x)}{x} \tag{A.56}$$

which makes:

$$\mathscr{F}\left[\Pi\left(\frac{t}{T}\right)\right] = T \cdot \text{sinc}(\pi \cdot T \cdot f) \tag{A.57}$$

Note that the definition of a Dirac impulse sometimes uses this rectangular pulse:

$$\delta(t) = \lim_{T \to 0} \frac{1}{T} \cdot \Pi\left[\frac{t}{T}\right] \tag{A.58}$$

It is easy to confirm that the properties mentioned above indeed hold for this definition.

A.3.4 A Triangular Pulse

The triangular function is defined as follows.

Definition A.13 Let $\Lambda[\cdot]$ denote the triangular function:

$$\Lambda\left[\frac{t}{T}\right] \triangleq \begin{cases} 1 - \frac{|t|}{T}, & |t| \leq T \\ 0, & |t| > T \end{cases} \tag{A.59}$$

The Fourier transform of this function is equal to:

$$\mathscr{F}\left[\Lambda\left(\frac{t}{T}\right)\right] = T \cdot \text{sinc}(\pi \cdot T \cdot f)^2 \tag{A.60}$$

Indeed, a triangular pulse can be constructed by the convolution of two rectangular pulses. Also this function is sometimes used to define the Dirac impulse:

$$\delta(t) = \lim_{T \to 0} \frac{1}{T} \cdot \Lambda\left[\frac{t}{T}\right] \tag{A.61}$$

A.3.5 The Derivative Triangular Pulse

A last function is the derivative of the triangular pulse. It is defined as:

Definition A.14 Let $\Xi[\cdot]$ denote the derivative triangular function:

$$\Xi\left[\frac{t}{T}\right] \triangleq \begin{cases} \frac{1}{T}, & T \leq t \leq 0 \\ \frac{-1}{T}, & 0 < t \leq T \\ 0, & |t| > T \end{cases} \tag{A.62}$$

The Fourier transform of this function is equal to:

$$\mathscr{F}\left[\Xi\left(\frac{t}{T}\right)\right] = 2 \cdot T \cdot \frac{\sin(\pi \cdot T \cdot f)^2}{-j \cdot \pi \cdot T \cdot f} \tag{A.63}$$

Appendix B
Influence of a Nonlinear Amplifier

This appendix explains some parts of the discussion in Sect. 4.2 on the influence of a nonlinear amplifier on the frequency of a harmonic oscillator. Especially the lengthy mathematical derivations are omitted in the text and derived here.

B.1 Derivation of Eq. (4.37)

In Sect. 4.2 it is shown that when the applied current waveform is known, the resulting frequency shift for a certain feedback network is given by (4.27):

$$\Im\left[Z_1\right] + \sum_{2}^{\infty} \Im\left[k \cdot Z_k\right] \cdot \delta_k^2 = 0 \tag{B.1}$$

where $\delta_k = I_k / I_1$ is the ratio of the harmonics and the fundamental component of the applied current. Z_k is the impedance of the tuned feedback network at the frequency $k \cdot \omega_0$ where ω_0 is the fundamental angular frequency of the oscillator. Assume a parallel RLC network with transfer function (2.66):

$$H_P(s) = \frac{\frac{s}{C}}{s^2 + \frac{1}{C \cdot R_P} \cdot s + \frac{1}{L \cdot C}} = \frac{\omega_n \cdot \sqrt{\frac{L}{C}} \cdot s}{s^2 + \frac{\omega_n}{Q} \cdot s + \omega_n^2} \tag{B.2}$$

When substituting $s = j \cdot k \cdot \omega_0$, the imaginary part of the resulting impedance is equal to:

$$\Im[Z_k] = \frac{-k \cdot \omega_0 \cdot Q^2 \cdot (k^2 \cdot \omega_0^2 - \omega_n^2)}{C \cdot (k^4 \cdot \omega_0^4 \cdot Q^2 - 2 \cdot k^2 \cdot Q^2 \cdot \omega_0^2 \cdot \omega_n^2 + \omega_n^4 \cdot Q^2 + k^2 \cdot \omega_0^2 \cdot \omega_n^2)} \tag{B.3}$$

V. De Smedt et al., *Temperature- and Supply Voltage-Independent Time References for Wireless Sensor Networks*, Analog Circuits and Signal Processing 128,
DOI 10.1007/978-3-319-09003-0

When $k = 1$, this equation simplifies to:

$$\Im[Z_1] = \frac{-\omega_0 \cdot Q^2 \cdot (\omega_0 + \omega_n) \cdot (\omega_0 - \omega_n)}{C \cdot (\omega_0^4 \cdot Q^2 - 2 \cdot Q^2 \omega_0^2 \cdot \omega_n^2 + \omega_n^4 \cdot Q^2 + \omega_0^2 \cdot \omega_n^2)} \tag{B.4}$$

$$= \frac{-\omega_0 \cdot Q^2 \cdot (\omega_0 + \omega_n) \cdot \Delta\omega_0}{C \cdot (\omega_0^4 \cdot Q^2 - 2 \cdot Q^2 \omega_0^2 \cdot \omega_n^2 + \omega_n^4 \cdot Q^2 + \omega_0^2 \cdot \omega_n^2)} \tag{B.5}$$

where $\Delta\omega_0 = \omega_0 - \omega_n$. Apart from the factor $\Delta\omega_0$, which is close to zero, it can be assumed that $\omega_0 \approx \omega_n$:

$$\Im[Z_1] \approx \frac{2 \cdot Q^2 \cdot \Delta\omega_0}{C \cdot \omega_n^2} \tag{B.6}$$

When $k \neq 1$, it can also be assumed that $\omega_0 \approx \omega_n$:

$$\Im[Z_k] = \frac{-k \cdot \omega_n^3 \cdot Q^2 \cdot (k^2 - 1)}{C \cdot (k^4 \cdot \omega_n^4 \cdot Q^2 - 2 \cdot k^2 \cdot Q^2 \cdot \omega_n^4 + \omega_n^4 \cdot Q^2 + k^2 \cdot \omega_n^4)} \tag{B.7}$$

$$= \frac{-k \cdot (k^2 - 1)}{C \cdot \omega_n \cdot (\frac{k^2}{Q^2} + k^4 - 2 \cdot k^2 + 1)} \tag{B.8}$$

$$= \frac{-k \cdot (k^2 - 1)}{C \cdot \omega_n \cdot (\frac{k^2}{Q^2} + (k^2 - 1)^2)} \tag{B.9}$$

When $Q \gg 1$ this simplifies to:

$$\Im[Z_k] = \frac{-k \cdot (k^2 - 1)}{C \cdot \omega_n \cdot (k^2 - 1)^2} = \frac{-k}{C \cdot \omega_n \cdot (k^2 - 1)} \tag{B.10}$$

The estimated frequency deviation, using (4.27), results in Eq. (4.37):

$$\frac{\Delta\omega_0}{\omega_n} = -\frac{1}{2 \cdot Q^2} \cdot \sum_{k=2}^{\infty} \frac{k^2}{k^2 - 1} \cdot \delta_k^2 \tag{B.11}$$

B.2 Waveform in a Nonlinear Harmonic Oscillator

In this section the waveform of a harmonic oscillator with a softly nonlinear amplifier is calculated. This, however, is not an easy task. Instead of the linear oscillator in Fig. B.1a, an oscillator with a linear feedback network (which is mostly the case) and with a nonlinear amplifier is studied, Fig. B.1b. The representation of this oscillator, using s-functions, is not correct since the amplifier is no longer a linear building block.

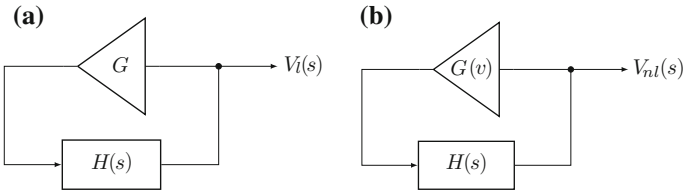

Fig. B.1 Typical block diagram of a harmonic (linear) oscillator (**a**). An oscillator with a linear feedback network and a nonlinear amplifier (**b**)

Similar to the calculations in Sect. 4.2.2, the calculations start with the Fourier series of the nonlinear, but periodic, output waveform:

$$v(t) = \sum_{k=-\infty}^{+\infty} c_k \cdot e^{j \cdot k \cdot \omega_0 \cdot t} \tag{B.12}$$

where, for real waveforms, $c_{-k} = \overline{c_k}$ and ω_0 is the fundamental frequency. This expression will be used to calculate the output current of the transconductance amplifier, which is the input current of the feedback network.

B.2.1 The Feedback Network

This waveform results from the injection of a current into the feedback network $H(s)$. Since the feedback network is assumed to be completely linear, the injected current can easily be calculated by dividing each frequency component c_k of the output voltage by the complex impedance $H(s)$ of the feedback network:

$$V(s) = I(s) \cdot H(s) \tag{B.13}$$

$$\Rightarrow i(t) = \sum_{k=-\infty}^{+\infty} \frac{c_k}{H(j \cdot k \cdot \omega_0)} \cdot e^{j \cdot k \cdot \omega_0 \cdot t} \tag{B.14}$$

For a parallel RLC feedback network, the transfer function can be written as:

$$H(s) = \frac{\frac{s}{C}}{s^2 + \frac{\omega_n}{Q} \cdot s + \omega_n^2} \tag{B.15}$$

where ω_n is the natural frequency of the feedback network and Q represents the quality factor. Since, for the steady-state behavior of the network:

$$1/H(j \cdot k \cdot \omega_0) = \left[j \cdot k \cdot \omega_0 \cdot C + \frac{\omega_n \cdot C}{Q} + \frac{C \cdot \omega_n^2}{j \cdot k \cdot \omega_0} \right] \tag{B.16}$$

$$= \frac{\omega_n \cdot C}{Q} \cdot \left[1 + j \cdot \left(\frac{k \cdot \omega_0 \cdot Q}{\omega_n} - \frac{Q \cdot \omega_n}{k \cdot \omega_0} \right) \right] \tag{B.17}$$

when the frequency deviation due to the nonlinearity of the amplifier is small compared to the natural frequency ω_n, this results in:

$$\frac{1}{H(j \cdot k \cdot \omega_0)} \approx \frac{\omega_n \cdot C}{Q} \cdot \left[1 + j \cdot k \cdot Q \left(1 - \frac{1}{k^2} \right) \right] \tag{B.18}$$

$$= \frac{\omega_n \cdot C}{Q} \cdot \sqrt{1 + k^2 \cdot Q^2 \cdot \left(1 - \frac{1}{k^2} \right)^2} \cdot e^{j \arctan(kQ(1-1/k^2))} \tag{B.19}$$

The complex impedance (conductance) experienced by each harmonic can be calculated with this formula.

B.2.2 The Nonlinear Amplifier

Another relationship between the voltage over the feedback network and the injected current is the amplifier characteristic. Although the Barkhausen criterion (Theorem 2.2) is only valid for linear systems, similar conclusions can be drawn for nonlinear systems. Since it is assumed that the oscillator's output signal is periodic and has a stable amplitude, the current-voltage relationship of both the feedback network and the amplifier must be the same! This equality results in, similar to what the Barkhausen criterion does for linear systems, the oscillator equation:

$$G(v(t)) = i(t) = \sum_{k=-\infty}^{+\infty} \frac{c_k}{H(j \cdot k \cdot \omega_0)} \cdot e^{j \cdot k \cdot \omega_0 \cdot t} \tag{B.20}$$

Solving this equation, if possible, results in the steady-state waveform of the oscillator. Note that startup behavior and transition effects are not taken into account in this equation. An amplifier with the following transfer characteristic is assumed:

$$G(v) = A_1 \cdot v + A_3 \cdot v^3 \tag{B.21}$$

where A_1 and A_3 are real coefficients determining the gain and nonlinearity of the amplifier and v is the input voltage. In order to obtain a stable output waveform, limited by the nonlinearity in the amplifier, A_1 must be positive and A_3 negative. Furthermore, to guarantee the startup of the oscillator, the gain for small input signals A_1 needs to compensate for the attenuation in the tank around the oscillation frequency ω_0. This amplifier characteristic, which is perfectly symmetric, is typical for differential circuits. It results in only odd harmonics in the output waveform.

B.2.2.1 Signals with an Infinite Bandwidth

In a first attempt to calculate the resulting waveform, one can try to insert the Fourier series of the voltage output signal into the amplifier characteristic. This, however, results in an infinite sum of cross products which is rather difficult to handle:

$$G(v(t)) = A_1 \cdot \sum_{k=-\infty}^{+\infty} c_k \cdot e^{j\cdot k\cdot \omega_0 \cdot t} + A_3 \cdot \sum_{k=-\infty}^{+\infty} c_k^3 \cdot e^{j\cdot 3\cdot k\cdot \omega_0 \cdot t} \tag{B.22}$$

$$+ 3 \cdot A_3 \cdot \sum_{k=-\infty}^{+\infty} \left\{ c_k \cdot e^{j\cdot k\cdot \omega_0 \cdot t} \cdot \sum_{l=-\infty}^{+\infty, l\neq k} c_l^2 \cdot e^{j\cdot 2\cdot k\cdot \omega_0 \cdot t} \right\} \tag{B.23}$$

This means that an infinite set of equations is needed to be solved to obtain all Fourier coefficients c_k. An alternative method is calculating the coefficients numerically in an iterative way. As will be shown, however, limiting the bandwidth of the output signal results in a solution with an acceptable accuracy.

B.2.2.2 Bandwidth-Limited Signals

A smarter approach is to assume that the output signal is band limited. A periodic voltage waveform, containing only the first, third and fifth harmonic, is assumed:

$$v(t) = \sum_{k=-5,-3,\ldots 5} c_k \cdot e^{j\cdot k\cdot \omega_0 \cdot t} \tag{B.24}$$

$$\begin{aligned}
G(v(t)) = {} & A_3 \cdot \overline{c_5}^3 \cdot e^{-15\cdot \omega_0 \cdot t} + 3 \cdot A_3 \cdot \overline{c_3} \cdot \overline{c_5}^2 \cdot e^{-13\cdot j\cdot \omega_0 \cdot t} \\
& + 3 \cdot A_3 \cdot (\overline{c_3}^2 \cdot \overline{c_5} + \overline{c_1} \cdot \overline{c_5}^2) \cdot e^{-11\cdot j\cdot \omega_0 \cdot t} \\
& + A_3 \cdot (\overline{c_3}^3 + 3 \cdot c_1 \cdot \overline{c_5}^2) \cdot e^{-9\cdot j\cdot \omega_0 \cdot t} \\
& + 3 \cdot A_3 \cdot (\overline{c_1}^2 \cdot \overline{c_5} + \overline{c_1} \cdot \overline{c_3}^2 + c_3 \cdot \overline{c_5}^2) \cdot e^{-7\cdot j\cdot \omega_0 \cdot t} \\
& + [A_1 \cdot \overline{c_5} + 3 \cdot A_3 \cdot (\overline{c_1}^2 \cdot \overline{c_3} + c_1 \cdot \overline{c_3}^2 + c_5 \cdot \overline{c_5}^2)] \cdot e^{-5\cdot j\cdot \omega_0 \cdot t} \\
& + [A_1 \cdot \overline{c_3} + A_3 \cdot \overline{c_1}^3 + 3 \cdot A_3 \cdot (c_1^2 \cdot \overline{c_5} + c_3 \cdot \overline{c_3}^2)] \cdot e^{-3\cdot j\omega_0 \cdot t} \\
& + [A_1 \cdot \overline{c_1} + 3 \cdot A_3 \cdot (c_1 \cdot \overline{c_1}^2 + \overline{c_3}^2 \cdot c_5)] \cdot e^{-1\cdot j\cdot \omega_0 \cdot t} \\
& + [A_1 \cdot c_1 + 3 \cdot A_3 \cdot (\overline{c_1} \cdot c_1^2 + c_3^2 \cdot \overline{c_5})] \cdot e^{1\cdot j\cdot \omega_0 \cdot t} \\
& + [A_1 \cdot c_3 + A_3 \cdot c_1^3 + 3 \cdot A_3 \cdot (\overline{c_1}^2 \cdot c_5 + \overline{c_3} \cdot c_3^2)] \cdot e^{3\cdot j\omega_0 \cdot t} \\
& + [A_1 \cdot c_5 + 3 \cdot A_3 \cdot (c_1^2 \cdot c_3 + \overline{c_1} \cdot c_3^2 + \overline{c_5} \cdot c_5^2)] \cdot e^{5\cdot j\cdot \omega_0 \cdot t} \\
& + 3 \cdot A_3 \cdot (c_1^2 \cdot c_5 + c_1 \cdot c_3^2 + \overline{c_3} \cdot c_5^2) \cdot e^{7\cdot j\cdot \omega_0 \cdot t} \\
& + A_3 \cdot (c_3^3 + 3 \cdot \overline{c_1} \cdot c_5^2) \cdot e^{9\cdot j\cdot \omega_0 \cdot t} \\
& + 3 \cdot A_3 \cdot (c_3^2 \cdot c_5 + c_1 \cdot c_5^2) \cdot e^{11\cdot j\cdot \omega_0 \cdot t} \\
& + 3 \cdot A_3 \cdot c_3 \cdot c_5^2 \cdot e^{13\cdot j\cdot \omega_0 \cdot t} + A_3 \cdot c_5^3 \cdot e^{15\cdot \omega_0 \cdot t}
\end{aligned} \tag{B.25}$$

where $\overline{x}$ is the complex conjugate of x. Since the signals in the oscillator are real signals, $c_{-k} = \overline{c_k}$. It appears from this expression that in the real system *all* odd

harmonics will be present due to the up-conversion in the nonlinear network. However, except for the harmonics from −5 to 5, higher harmonics are neglected in this derivation. Since the current input of the feedback network is assumed to be equal to the output of the amplifier, using (B.19), this results in 3 independent complex equations. Due to the fact the signals are real, the complex conjugate equations can be left out:

$$c_1 \cdot \frac{\omega_0 \cdot C}{Q} = [A_1 \cdot c_1 + 3 \cdot A_3 \cdot (\overline{c_1} \cdot c_1^2 + \overline{c_5} \cdot c_3^2)] \tag{B.26}$$

$$c_3 \cdot \frac{\omega_0 \cdot C}{Q} \cdot \sqrt{1 + 9 \cdot Q^2 \cdot \left(\frac{8}{9}\right)^2} \cdot e^{j \cdot \arctan\left(3 \cdot Q \cdot \frac{8}{9}\right)} = [A_1 \cdot c_3 + A_3 \cdot c_1^3 + 3 \cdot A_3 \cdot (c_5 \cdot \overline{c_1}^2 + \overline{c_3} \cdot c_3^2)] \tag{B.27}$$

$$c_5 \cdot \frac{\omega_0 \cdot C}{Q} \cdot \sqrt{1 + 25 \cdot Q^2 \cdot \left(\frac{24}{25}\right)^2} \cdot e^{j \cdot \arctan\left(5 \cdot Q \cdot \frac{24}{25}\right)} = [A_1 \cdot c_5 + 3 \cdot A_3 \cdot (c_3 \cdot c_1^2 + \overline{c_1} \cdot c_3^2 + \overline{c_5} \cdot c_5^2)] \tag{B.28}$$

This set of equations can be solved for a certain feedback network and amplifier in order to obtain the output waveform. The bandwidth limitation of the signal, however, requires a careful approach, certainly for a high gain in the amplifier and/or networks with a low Q factor. A high Q results in a sharper peak in the transfer function; hence, this results in a suppression of the harmonics.

B.2.3 Application to a Known Network

Let us illustrate this now with an example. Suppose an oscillator with a feedback network similar to Fig. 2.9a (a parallel RLC-tank). The resonant angular frequency is normalized and therefore equal to 1 rad/s. The Q-factor is assumed to be equal to 10. The transfer function then looks as follows:

$$H(s) = \frac{s/C}{s^2 + \frac{1}{10} \cdot s + 1} \tag{B.29}$$

At the resonant frequency, this transfer function is a real function with a value of (B.19):

$$H(j \cdot \omega_n) = \frac{Q}{\omega_n \cdot C} = \frac{10}{C} \tag{B.30}$$

which means that the higher the value of the capacitor in the network (for a certain resonant frequency and Q-factor), the lower the impedance at resonance. Note that, using $\omega_n = 1/\sqrt{L \cdot C}$ and $Q = R_P \cdot \sqrt{C/L}$ (2.64), this equation equals R_P. For the sake of keeping the problem simple and understandable, the value of the capacitor is chosen equal to 10, which makes the impedance of the network 1 at the resonant

frequency. This means that the gain of a linear amplifier must also be equal to 1, according to Barkhausen. Therefore, the following characteristic is assumed:

$$G(v) = 1.1 \cdot v - 0.1 \cdot v^3 \tag{B.31}$$

This means, for an input voltage of ±1 V, that the gain indeed decreases to 1. As a result, an output amplitude slightly higher than 1 V is expected. Solving the oscillator Eqs. (B.26–B.28), results in the following solution:

$$c_1 = 2.0301 \times 10^{-1} + j \cdot 5.4048 \times 10^{-1} \tag{B.32}$$

$$c_3 = 4.5033 \times 10^{-6} - j \cdot 7.6881 \times 10^{-6} \tag{B.33}$$

$$c_5 = -1.8225 \times 10^{-8} + j \cdot 3.5200 \times 10^{-9} \tag{B.34}$$

It is clearly visible that the impact of the harmonics in the resulting signal is low compared to the fundamental waveform. This, however, changes when the (small-signal) gain, A_1, becomes higher. The resulting coefficients for different values of the gain are shown in Table B.1. Because of the 'soft' distortion in the amplifier, the influence on the frequency is rather low. The case of an amplifier with strong distortion is discussed in Sect. 4.2.2. The waveform of the output voltage over the tank and the output current of the amplifier are shown in Fig. B.2. In this figure, the impact of the nonlinearity is clearly visible in the applied current. The resonant feedback network, however, hides most of these nonlinearities in the output voltage signal.

Note that this method to calculate the harmonics in the output waveform starts from the assumption that the center frequency is fixed. By doing this, one degree of freedom is taken away in the set of equations. When the frequency is left as a variable, another variable (such as the initial phase shift of the fundamental frequency) has to be chosen freely. Furthermore, due to this assumption, this method only works for circuits with a limited amount of harmonics. Increasing the number of harmonics in the output waveform increases the accuracy but also causes an explosion of terms in the output waveform.

B.3 Proof of Eq. (4.42)

The sum of the infinite series in Sect. 4.2.2 can be written as:

$$\sum_{k\in\{3,5,\ldots\}}^{\infty} \frac{1}{k^2-1} = \sum_{k=1}^{\infty} \frac{1}{(2\cdot k+1)^2-1} \tag{B.35}$$

$$= \frac{1}{4} \cdot \sum_{k=1}^{\infty} \frac{1}{k\cdot(k+1)} \tag{B.36}$$

The sum can be calculated using the following formula:

Table B.1 Coefficients of the different harmonics of the output waveform for the example oscillator

	$Q = 10$	$Q = 1$
$i(v) = 1.1 \cdot v - 0.1 \cdot v^3$		
c_1	$2.030 \times 10^{-1} + j \cdot 5.405 \times 10^{-1}$	$4.638 \times 10^{-1} + j \cdot 3.438 \times 10^{-1}$
c_3	$4.503e-6 - j \cdot 7.688e-6$	$-2.156 \times 10^{-5} - j \cdot 1.816 \times 10^{-5}$
c_5	$-1.823e-8 + j \cdot 3.520e-9$	$1.611 \times 10^{-7} - j \cdot 9.622 \times 10^{-8}$
$\Delta\omega_0/\omega_n$	-3.572×10^{-10}	-3.577×10^{-9}
$i(v) = 1.3 \cdot v - 0.1 \cdot v^3$		
c_1	$5.676 \times 10^{-1} - j \cdot 8.233 \times 10^{-1}$	$4.314 \times 10^{-1} - j \cdot 9.022 \times 10^{-1}$
c_3	$1.265 \times 10^{-5} - j \cdot 4.454 \times 10^{-5}$	$1.816 \times 10^{-5} - j \cdot 1.454 \times 10^{-4}$
c_5	$-2.692 \times 10^{-8} - j \cdot 2.881 \times 10^{-7}$	$-1.231 \times 10^{-6} - j \cdot 2.658 \times 10^{-6}$
$\Delta\omega_0/\omega_n$	-3.215×10^{-9}	-3.223×10^{-8}
$i(v) = 1.5 \cdot v - 0.1 \cdot v^3$		
c_1	$4.601 \times 10^{-1} + j \cdot 1.206 \times 10^{0}$	$-6.181 \times 10^{-1} + j \cdot 1.133 \times 10^{0}$
c_3	$4.901 \times 10^{-5} - j \cdot 8.673 \times 10^{-5}$	$-8.824 \times 10^{-5} + j \cdot 3.026 \times 10^{-4}$
c_5	$-1.012 \times 10^{-6} + j \cdot 2.314 \times 10^{-7}$	$1.896 \times 10^{-6} + j \cdot 1.035 \times 10^{-5}$
$\Delta\omega_0/\omega_n$	-8.934×10^{-9}	-8.971×10^{-8}
$i(v) = 2.0 \cdot v - 0.1 \cdot v^3$		
c_1	$-6.213 \times 10^{-1} + j \cdot 1.717 \times 10^{0}$	$7.372 \times 10^{-1} - j \cdot 1.670 \times 10^{0}$
c_3	$1.332 \times 10^{-4} + j \cdot 2.483 \times 10^{-4}$	$2.870 \times 10^{-5} - j \cdot 8.913 \times 10^{-4}$
c_5	$5.772 \times 10^{-6} + j \cdot 1.059 \times 10^{-6}$	$-3.532 \times 10^{-5} - j \cdot 4.815 \times 10^{-5}$
$\Delta\omega_0/\omega_n$	-3.577×10^{-8}	-3.622×10^{-7}

Also the influence of the harmonics on the center frequency is shown in the table

Theorem B.1

$$\sum_{k=1}^{l} \frac{1}{k \cdot (k+1)} = \frac{l}{l+1} \tag{B.37}$$

Proof This proof uses induction: first it is shown that the explicit formula holds for $l = 1$; afterwards it is shown that, if the formula holds for l, it will also hold for $l+1$.

- $l = 1$
  It can easily be seen that:

$$\sum_{k=1}^{l=1} \frac{1}{k \cdot (k+1)} = 1/2 = \frac{l}{l+1} \tag{B.38}$$

- $l + 1$
  When the formula holds for l, the sum of the series from 1 to $l+1$ can be written as:

$$\sum_{k=1}^{l+1} \frac{1}{k \cdot (k+1)} = \sum_{k=1}^{l} \frac{1}{k \cdot (k+1)} + \frac{1}{(l+1) \cdot (l+2)} \tag{B.39}$$

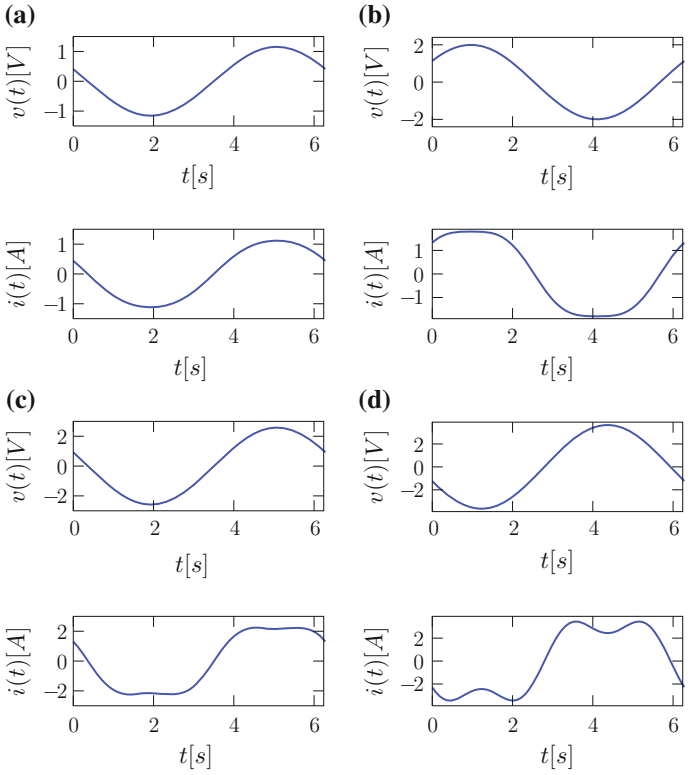

Fig. B.2 Output voltage waveform and injected current for different transconductance amplifiers with soft distortion. The nonlinearity is necessary to control the amplitude but causes harmonics in the output waveform. The harmonics, on their turn, cause a small frequency drop. **a** $Q = 10$, $i(v) = 1.5 \cdot v - 0.1 \cdot v^3$. **b** $Q = 10$, $i(v) = 2.0 \cdot v - 0.1 \cdot v^3$

$$= \frac{l}{l+1} + \frac{1}{(l+1)\cdot(l+2)} \tag{B.40}$$

$$= \frac{l^2 + 2\cdot l + 1}{(l+1)\cdot(l+2)} \tag{B.41}$$

$$= \frac{l+1}{l+2} \tag{B.42}$$

which proves Theorem B.1. ■

It can easily be seen that:

$$\lim_{l\to+\infty} \sum_{k=1}^{l} \frac{1}{k\cdot(k+1)} = \lim_{l\to+\infty} \frac{l}{l+1} = 1 \tag{B.43}$$

which is used to obtain the result of (4.42).

Appendix C
Measurement Issues for Jitter and Phase Noise

Measuring jitter and phase noise in an oscillator output signal is a difficult task. It is mainly the colored noise which complicates the measurements because of the ultra-slow frequency variations, which causes frequency drift. A possible consequence of this, when measuring the cycle-to-cycle jitter, is that the subsequent measurements do not converge! Due to the frequency drift, the measured period 'drifts away' from the average period depending on the moment at which the measurement is performed. In [92, 180] different methods are discussed to overcome these problems.

C.1 White Noise Jitter Divergence

Different measures are available to express the instabilities in an oscillator output signal. Most of them are based on the *variance* of variations in the frequency, phase or phase-time. The phase deviation $\phi(t)$ of an oscillator modulated with white noise is given by a *random walk* about the ideal phase $\omega_0 \cdot t$ (the resulting PSD is proportional to $1/f^2$). When considering the variance σ_ϕ of the phase fluctuations, this causes a continuous increase with the observation time (this is similar to the absolute jitter, Definition 3.1; the uncertainty of the next clock edge will increase over time). This can be understood by the knowledge that the VCO is an ideal integrator, of which the output (the phase) can grow forever. It is this very same integration that shapes the PSD of the phase fluctuations $S_\phi(f)$, which makes the PSD go to infinity. This integration operation is the same as the so-called superposition integral in Hajimiri's theory, Eq. (3.20).

To bound this error, the VCO can be put in a phase-locked loop (PLL), which limits the phase deviation compared to a reference clock. In the time domain, this can be interpreted as a periodical *reset* of the phase deviation. In the frequency domain, this means that the low-frequency content of the output phase deviation is filtered. The transfer function of a PLL acts as a high-pass filter on the oscillator output. In this configuration, the jitter can easily be measured, because it does not drift away from the ideal (reference) phase. Furthermore this technique allows to measure

V. De Smedt et al., *Temperature- and Supply Voltage-Independent Time References for Wireless Sensor Networks*, Analog Circuits and Signal Processing 128,
DOI 10.1007/978-3-319-09003-0

the frequency deviation of the oscillator by means of the VCO input signal, which is proportional to the frequency deviation between the oscillator and the reference input. The carrier frequency is not present in this control signal, which allows to exploit the full dynamic range of the measurement setup (if a strong carrier signal is present, the phase noise or frequency is dominated by the carrier signal). The main drawback of this *closed-loop, clock-referenced* technique is the fact the output is filtered by the PLL transfer function, which needs to be corrected afterwards [92, 180, 181].

Another method to avoid the divergence of frequency stability measures in the time domain is limiting the time interval over which they are measured. So-called *open-loop, self-referenced* techniques [180] start a measurement at a certain clock edge and measure the jitter of the following clock edges compared to the first clock edge. When starting a new measurement, ($t = 0$) the phase error is reset. In this way, the phase error can only drift away during the measurement interval. When the jitter of the subsequent clock cycles is uncorrelated, the following standard deviation as a function of the measurement interval t can be expected (3.59):

$$\sigma_{abs,OL}(t) = \sqrt{c} \cdot \sqrt{t} \tag{C.1}$$

which is equivalent to Eq. (3.59) and valid when only white noise is injected in the oscillator ($1/f^2$ in the oscillator spectrum). This means that the cycle-to-cycle jitter is an open-loop, self-referenced jitter measurement for which the measurement time is equal to the oscillator period, $t = 1/f_{osc}$. c is an important Figure of Merit of an oscillator, which is related to the shape of the Lorentzian noise spectrum (3.50). Although the cycle-to-cycle jitter is a straightforward measurement to quantify the phase noise, a high time resolution or a specialized measurement setup is needed to do these measurements [92]. An interesting question is how both measurements, *closed-loop* and *open-loop*, can be related.

The measured jitter of a closed-loop measurement strongly depends on the bandwidth of the PLL. In [180] it is illustrated that, for a PLL of which the transfer function can be approximated by the low-pass characteristic:

$$H(s) = \frac{2 \cdot \pi \cdot f_L}{s + 2 \cdot \pi \cdot f_L} \tag{C.2}$$

where f_L is the loop bandwidth of the PLL, the measured jitter stabilizes when the measurement time is high compared to $1/(2 \cdot \pi \cdot f_L)$. This can be understood as follows: when performing a self-referenced measurement starting at $t = 0$, the jitter increases with the square root of the measurement interval. At the moment the measurement time approaches

$$t_L = \frac{1}{2 \cdot \pi \cdot f_L}, \tag{C.3}$$

the PLL is able to compensate for higher phase deviations and the jitter becomes constant as a function of time. When the absolute jitter of a clock edge, compared

to the reference clock, is called σ_x, than the jitter between two clock edges, which are separated a period $\Delta t \gg t_L$ from each other, is equal to $\sqrt{2} \cdot \sigma_x$, assuming that this jitter is uncorrelated. In [180, 282] this characteristic, which is a function of the PLL bandwidth f_L, is analyzed. It is shown that:

$$\sigma_x = \sqrt{c} \cdot \sqrt{\frac{1}{4 \cdot \pi \cdot f_L}} \tag{C.4}$$

Indeed: the resulting jitter is a factor $\sqrt{2}$ different from the jitter at the -3 dB $(=1/\sqrt{2})$ bandwidth f_L of the PLL. These conclusions are important when performing the *closed-loop, clock-referenced* measurement discussed earlier to compensate for the PLL behavior. The jitter can be reduced in two ways: by improving the oscillator jitter (c) and by increasing the PLL bandwidth (f_L). This clearly shows the relationship between a closed-loop and an open-loop measurement.

C.1.1 Frequency Fluctuations as a Noise Measure

The instantaneous relative frequency fluctuations are represented by (2.41):

$$y(t) = \frac{\frac{d\phi(t)}{dt}}{\omega_0} \tag{C.5}$$

As a matter of fact, the frequency cannot be measured instantaneously (opposite to phase measurements, in the absence of amplitude noise), which makes it necessary to measure the frequency drift over a certain time span τ:

$$\langle y \rangle_{t_0,\tau} = \frac{1}{\tau} \cdot \int_{t_0-\tau/2}^{t_0+\tau/2} y(t)dt. \tag{C.6}$$

Using (2.41), this equation can be written as:

$$\langle y \rangle_{t_0,\tau} = \frac{\phi(t_0 + \tau/2) - \phi(t_0 - \tau/2)}{\omega_0 \cdot \tau} = \frac{1}{\tau} \cdot [x(t_0 + \tau/2) - x(t_0 - \tau/2)] \tag{C.7}$$

This means that the averaged instantaneous frequency fluctuations over a certain time interval can be calculated as the normalized phase-time $x(t)$ error over the very same time interval. Since $y(t)$, $\phi(t)$ and therefore also $x(t)$ are random processes, this averaged error is a random variable with a mean value and a standard deviation. The mean value is equal to zero, which makes the variance equal to the mean-square value:

$$\sigma^2_{\langle y \rangle,\tau} = E[\langle y \rangle^2_{t_0,\tau}] \tag{C.8}$$

where $E[\cdot]$ stands for the expected value calculated over an infinite set of samples. It can therefore be stated that $\sigma^2_{\langle y\rangle,\tau}$ is the true variance of $\langle y\rangle_{t_0,\tau}$. In a practical situation, however, it is not possible to create an infinite set of samples, which makes the variance itself a random variable over the different (limited) sample sets. It is considered to be an estimator for the true variance (based on a limited set). A good, unbiased, estimator is an estimator of which the average value converges to the true variance. An unbiased estimator for the variance is given by:

$$s^2_{\langle y\rangle,\tau} = \frac{1}{N-1} \cdot \sum_{i=1}^{N} \left(\langle y\rangle_{t_i,\tau} - \frac{1}{N} \cdot \sum_{j=1}^{N} \langle y\rangle_{t_j,\tau} \right)^2 \tag{C.9}$$

where N is the number of samples of $\langle y\rangle$ in the subset and $N \geq 2$ [217]. This estimator holds as long as the samples are uncorrelated. Note also the difference in notation between the true variance of an infinite set σ^2_x and the estimated variance of a subset s^2_x. The relationship between this variance and the cycle-to-cycle jitter is:

$$\sigma_{\langle y\rangle,T_0} = \frac{\sigma_c}{T_0} \tag{C.10}$$

C.1.2 Relation Between the Variance and the PSD

The link between the PSD and the variance of the fractional frequency fluctuations is obtained by considering the fact that the time interval τ over which the frequency fluctuations are averaged, can be treated as a filter in the time domain. In this way, the samples of $\langle y\rangle_{t_0,\tau}$ are considered to be a moving average operation:

$$\langle y\rangle_{t_0,\tau} = \frac{1}{\tau} \cdot \int_{t_0-\tau/2}^{t_0+\tau/2} y(t)dt \tag{C.11}$$

$$= \frac{1}{\tau} \cdot \int_{-\infty}^{\infty} y(t) \cdot \Pi\left(\frac{t}{\tau}\right) dt \tag{C.12}$$

$$= \frac{1}{\tau} \cdot \int_{-\infty}^{\infty} y(t) \cdot \Pi\left(\frac{t_0 - t}{\tau}\right) dt \tag{C.13}$$

which is a convolution integral. The variance is then obtained by integrating over the PSD of the resulting waveform:

$$\sigma^2_{\langle y \rangle,\tau} = \int_{-\infty}^{\infty} S_y(f) \cdot \left(\frac{\sin(\pi \cdot f \cdot \tau)}{\pi \cdot f \cdot \tau} \right)^2 df \tag{C.14}$$

$$= \int_{-\infty}^{\infty} \frac{f^2}{f_0^2} \cdot S_\phi(f) \cdot \left(\frac{\sin(\pi \cdot f \cdot \tau)}{\pi \cdot f \cdot \tau} \right)^2 df \tag{C.15}$$

where the factor $\left(\frac{\sin(\pi \cdot f \cdot \tau)}{\pi \cdot f \cdot \tau} \right)^2$ is called the *transfer function of the time-domain measure of frequency stability* [92, 217]. Using (C.10) it can be seen that this equation is equivalent to (3.67). In case of a $1/f^2$ phase noise profile, this integral will converge.

The previous discussion assumes white, uncorrelated noise. In Sect. 3.6 it has been shown that in the case of correlated or colored noise sources, the linear increase over time for an open-loop measurement does not hold. Only measuring the jitter over a certain time interval to obtain the cycle-to-cycle jitter, is therefore not sufficient to do a jitter characterization. In the frequency domain, this is comparable to characterizing the noise based on only one frequency value of the PSD. The influence of the frequency noise shaping ($1/f^\alpha$) is closely related to the evolution of the absolute jitter over time (3.65).

C.2 Colored Noise Jitter

When colored noise is injected in an oscillator, this results in an $1/f^\alpha$ region in the phase spectrum. α is in this case greater or equal to 3. In this case, the absolute jitter does no longer increase proportionally to the square root of the observation time, but also a term proportional to the observation time appears, (3.65). As explained in Sect. 3.6.3, the noise injected during subsequent time intervals is therefore correlated, which causes the phase to drift faster away than in the case of uncorrelated noise sources. As stated in [104], it can be assumed in this case that the standard deviation adds instead of the variance.

C.2.1 Frequency Fluctuations as a Colored Noise Measure

As previously shown, the fractional frequency fluctuations are an interesting measure to measure the frequency stability in the time domain. Moreover, due to its relation to the cycle-to-cycle jitter, it gives an intuitive insight in the behavior and the effects of the jitter on for instance the performance of a clocked circuit. Problems arise, however, when the integral (C.15) is calculated for a colored noise spectrum. Keeping in mind that the transfer function of the time-domain measure of frequency stability is equal to 1 around $f = 0$, it is clear that this integral will diverge, see (2.47) with

$\alpha \leq -1$. Typically, this is solved by limiting the minimum frequency to which this integral is calculated around the carrier. Often this is explained as a limit which comes forth from the limited observation time. This, however, is not satisfactory since the calculated variance strongly depends on this value and therefore does not converge when a larger observation time is used [41].

A solution can be to use the PLL measurement method described above: the frequencies within the bandwidth of the PLL, f_L, are suppressed as a result of the PLL feedback mechanism. In this way, as a result of the continuous tuning of the oscillator to the nominal frequency of the frequency reference, the variance of the frequency fluctuations (and the jitter) converges for an increasing number of samples $\langle y \rangle_{t_0,\tau}$ when the total observation time is larger than the inverse of the loop bandwidth [92].

C.2.2 The Allan Variance

A different way to overcome these convergence problems, is the use of an alternative measure instead of the variance. Instead of using the complete set of average frequency fluctuations $\langle y \rangle_{t_0,\tau}$, one can combine the subsequent averages instead. The Allan variance, which is also an IEEE-recommended measure for frequency stability, is defined as [5]:

$$\sigma^2_{A,\langle y \rangle,\tau} = E\left[\sum_{i=1}^{2}\left(\langle y \rangle_{t_i,\tau} - \frac{1}{2}\cdot\sum_{j=1}^{2}\langle y \rangle_{t_j,\tau}\right)^2\right] \tag{C.16}$$

$$= \frac{1}{2}\cdot E[(\langle y \rangle_{t_2,\tau} - \langle y \rangle_{t_1,\tau})^2] \tag{C.17}$$

where $\langle y \rangle_{t_i,\tau}$ is defined as:

$$\langle y \rangle_{t_i,\tau} = \frac{1}{\tau}\cdot\int_{t_i-\tau/2}^{t_i+\tau/2} y(t)dt \tag{C.18}$$

and $t_{i+1} - t_i = \tau$, which means that there is no *dead time* between the subsequent samples. Similar to (C.7), also this equation can be expressed in terms of the phase-time $x(t_k)$ (2.40):

$$\sigma^2_{A,\langle y \rangle,\tau} = \frac{1}{2\cdot\tau^2}\cdot E\left[[x(t_{k+2}) - 2\cdot x(t_{k+1}) + x(t_k)]^2\right] \tag{C.19}$$

which shows the tight connection between the Allan variance and the alternative definition of the cycle-to-cycle jitter, (3.62). Although the difference between the Allan variance and the classic variance is subtle, it has a huge impact on the correlated noise. The correlation between the subsequent samples is, due to the definition of the

Allan variance, canceled. The linear trend in the jitter is compensated by combining several samples. To demonstrate the convergence in case of a colored $(1/f)$ noise source, the transfer function of this frequency measure has to be determined. The Allan variance is the variance of the random variable:

$$\frac{1}{\sqrt{2}} \cdot (\langle y \rangle_{t_{k+1},\tau} - \langle y \rangle_{t_k,\tau}) = \frac{1}{\sqrt{2} \cdot \tau} \cdot \int_{-\infty}^{\infty} y(t) \cdot h_A \left(\frac{t_{k+1} - t}{\tau} \right) dt \tag{C.20}$$

where $h_A(t_{k+1} - t)$ is equal to the *derivative triangular function* (see definition A.14):

$$h_A(t) = \Xi(t/\tau) \triangleq \begin{cases} \frac{1}{\tau}, & \tau \leq t \leq 0 \\ \frac{-1}{\tau}, & 0 < t \leq \tau \\ 0, & |t| > \tau \end{cases} \tag{C.21}$$

The resulting PSD, after performing the filtering operation, can then be integrated to obtain the resulting Allan variance of the oscillator signal:

$$\sigma^2_{A,\langle y \rangle,\tau} = \int_{-\infty}^{\infty} S_y(f) \cdot 2 \cdot \left(\frac{\sin(\pi \cdot f \cdot \tau)^2}{\pi \cdot f \cdot \tau} \right)^2 df \tag{C.22}$$

$$= \int_{-\infty}^{\infty} \frac{f^2}{f_0^2} \cdot S_\phi(f) \cdot 2 \cdot \left(\frac{\sin(\pi \cdot f \cdot \tau)^2}{\pi \cdot f \cdot \tau} \right)^2 df \tag{C.23}$$

Because of the low-frequency filtering operation of the Allan variance, the integral is convergent also when $1/f$ noise is injected in the oscillator. However, an upper limit for the noise integration is still needed for white and flicker noise. Typically this bound is taken at the cutoff frequency f_h which is existing in each system. In a nonlinear oscillator, it is reasonable to integrate until 1.5 times the oscillation frequency; every higher frequency is also represented in this bandwidth. In Table C.1 an overview is given of the resulting Allan variance for different slopes of the frequency (phase) spectrum, as a function of the observation time τ. It is clearly seen that only for *flicker frequency fluctuations* the Allan variance is independent of the observation time.

An interesting conclusion after using the Allan variance is the observation that by combining measurements of subsequent periods, the low-frequency content can be filtered away. However, from Table C.1 it appears that the Allan variance is only able to compensate for the first-order colored noise contributions. In the following section, a methodology is demonstrated to also compensate for the higher-order contributions in order to quantify them in the time domain.

Table C.1 The Allan variance for different slopes of the (single-sided) PSD

$S_y(f)$	$S_\phi(f)$	$\sigma^2_{A,\langle y\rangle,\tau}$	Description
$h_{-2}\cdot f^{-2}$	$f_0^2\cdot h_{-2}\cdot f^{-4}$	$\frac{2\cdot\pi^2\cdot h_{-2}\cdot\tau}{3}$	Random walk frequency fluctuations
$h_{-1}\cdot f^{-1}$	$f_0^2\cdot h_{-1}\cdot f^{-3}$	$2\cdot\ln(2)\cdot h_{-1}$	Flicker frequency fluctuations
$h_0\cdot f^0$	$f_0^2\cdot h_0\cdot f^{-2}$	$\frac{h_0}{2\cdot\tau}$	White frequency fluctuations
$h_1\cdot f^1$	$f_0^2\cdot h_1\cdot f^{-1}$	$\frac{h_1}{4\cdot\pi^2\cdot\tau^2}\cdot[1.038+3\cdot\ln(2\cdot\pi\cdot f_h\cdot\tau)]$	Flicker phase fluctuations
$h_2\cdot f^2$	$f_0^2\cdot h_2\cdot f^0$	$\frac{3\cdot h_2\cdot f_h}{4\cdot\pi^2\cdot\tau^2}$	White phase fluctuations

It is clearly seen that only for $1/f$ noise injected in the oscillator, a constant value is obtained [5, 217]

C.2.3 The Use of Structure Functions

The use of structure functions in the area of oscillator phase noise analysis was first introduced by Lindsey and Chie [164]. It will be shown below that this theory succeeds in capturing the previously discussed time-domain noise measures (variances) in a unifying methodology. Structure functions are a mathematical tool which can be used to avoid the singularities which appear at low frequencies in the case of colored noise sources. The underlying idea is that the structure functions are able to de-trend the measurement data, similar to what the Allan variance does for first-order colored noise sources.

C.2.3.1 Increments of a Function

The increment of a random process $x(t)$ is defined as follows:

Definition C.1 Let $\Delta^N x(t,\tau)$ denote the N-th increment of $x(t)$ with time step τ. The first-order increment of a random process $x(t)$ is defined as:

$$\Delta^1 x(t,\tau) = x(t+\tau) - x(t) \tag{C.24}$$

The N-th-order increment of a function can recursively be defined as:

$$\Delta^N x(t,\tau) = \Delta^{N-1}[\Delta^1 x(t,\tau)] = \Delta^1[\Delta^{N-1}x(t,\tau)] \tag{C.25}$$

or can be written explicitly as:

$$\Delta^N x(t,\tau) = \sum_{k=0}^{N}(-1)^k\cdot\binom{N}{k}\cdot x[t+(N-k)\cdot\tau] \tag{C.26}$$

where $\binom{N}{k}$ denotes *the combinations of k samples out of N*.

Note that this definition results in the same formulas as used to approximate the N-th-order derivative of $x(t)$ using only forward differences. This observation helps to understand the working principle of this method. When calculating the N-th-order increment, $N+1$, τ-spaced samples of the function are needed. Moreover, when M, τ-spaced samples are available, $M-N$ N-th-order increments can be calculated, which results in a high data utilization for large numbers of samples. Because the adjacent samples are combined, the increments are able to detect or cancel trends or correlations between the different data points. Generally speaking, the *variance* of the result of a certain increment is larger for uncorrelated samples than for correlated data samples. This is the same working principle of the Allan variance for adjacent oscillation periods! Note that the N-th increment of a polynomial of an order smaller than N, is equal to zero. This corresponds to the fact that these increments are an estimator of the N-th derivative.

C.2.3.2 Structure Functions

Based on these increments, structure functions can be defined:

Definition C.2 The N-th-order structure function $D_x^N(t_s, \tau)$ is defined as the autocorrelation function of the N-th increment:

$$D_x^N(t_s, \tau) \triangleq \left\langle (\Delta^N x(t, \tau)) \cdot (\Delta^N x(t + t_s, \tau)) \right\rangle \tag{C.27}$$

$$= \lim_{T \to \infty} \int_{-T/2}^{T/2} (\Delta^N x(t, \tau)) \cdot (\Delta^N x(t + t_s, \tau) dt \tag{C.28}$$

When the time shift t_s is equal to zero, this can shortly be written as:

$$D_x^N(\tau) = \left\langle (\Delta^N x(t, \tau))^2 \right\rangle \tag{C.29}$$

In this work, the term *structure function* refers to the structure function with $t_s = 0$, which is in fact the variance of the N-th-order increment of $x(t)$. In [164] it is shown that these functions can easily be related to the output PSD of the oscillator [92].

$$D_x^N(\tau) = 2^{2 \cdot N} \cdot \int_{-\infty}^{\infty} S_x(f) \cdot \sin^{2 \cdot N}(\pi \cdot f \cdot \tau) df \tag{C.30}$$

$$D_x^N(\tau) = 2^{2 \cdot N - 2} \cdot \int_{-\infty}^{\infty} S_y(f) \cdot \frac{\sin^{2 \cdot N}(\pi \cdot f \cdot \tau)}{(\pi \cdot f)^2} df \tag{C.31}$$

$$\frac{D_x^N(\tau)}{\tau^2} = 2^{2 \cdot N - 2} \cdot \int_{-\infty}^{\infty} S_y(f) \cdot \frac{\sin^{2 \cdot N}(\pi \cdot f \cdot \tau)}{(\pi \cdot f \cdot \tau)^2} df \tag{C.32}$$

where the last equation is just the structure function normalized to the observation interval τ. These equations can be obtained by using the *gated integration* approach as previously demonstrated for the variance and the Allan variance. If f is close to zero, the transfer function of the timing measure can be approximated by:

$$|H_{D,N}(f)| = \left| \frac{\sin^N(\pi \cdot f \cdot \tau)}{(\pi \cdot f \cdot \tau)} \right| \approx (\pi \cdot f \cdot \tau)^{N-1} \tag{C.33}$$

This means that the singularities in the spectrum can be compensated by using the correct structure function. Since:

$$S_y(f) \cdot \frac{\sin^{2\cdot N}(\pi \cdot f \cdot \tau)}{(\pi \cdot f \cdot \tau)^2} \sim f^{\alpha} \cdot f^{2N-2} \tag{C.34}$$

the integration of the spectrum is convergent as long as $\alpha > -(2 \cdot N - 1)$ or $N > \frac{1-\alpha}{2}$. This indicates that it is always possible to take a high enough order of increment N to obtain a bounded structure function. The effect of taking a higher-order structure function is demonstrated in Table C.2. Interesting to note is the fact that the structure functions have a close relationship with the previously defined time-domain jitter measures:

$$\sigma^2_{\langle y \rangle, \tau} = \frac{1}{\tau^2} \cdot D^1_x(\tau) \tag{C.35}$$

$$\sigma^2_{A, \langle y \rangle, \tau} = \frac{1}{2 \cdot \tau^2} \cdot D^2_x(\tau) \tag{C.36}$$

C.2.3.3 Structure Functions to Measure Polynomial Drift

Colored or correlated noise sources result in a polynomial drift in for instance the phase-time error. It is interesting to compare the results of the random noise process

Table C.2 Values of the different structure functions, corresponding to the different areas in the power-law noise spectrum

$S_\phi(f)$	$D^1_x(\tau)$	$D^2_x(\tau)$	$D^3_x(\tau)$
$f_0^2 \cdot h_{-2} \cdot f^{-4}$	Non-convergent	$\frac{4}{3} \cdot \pi^2 \cdot h_{-2} \cdot \tau^3$	$2 \cdot \pi^2 \cdot h_{-2} \cdot \tau^3$
$f_0^2 \cdot h_{-1} \cdot f^{-3}$	Non-convergent	$4 \cdot \ln(2) \cdot h_{-1} \cdot \tau^2$	$6.75 \cdot h_{-1} \cdot \tau^2$
$f_0^2 \cdot h_0 \cdot f^{-2}$	$\frac{1}{2} \cdot h_0 \cdot \tau$	$h_0 \cdot \tau$	$3 \cdot h_0 \cdot \tau$
$f_0^2 \cdot h_1 \cdot f^{-1}$	$\frac{1}{2 \cdot \pi^2} \cdot h_1 \cdot [\ln(\pi \cdot \tau \cdot f_h) + 1.27]$	$\frac{3}{2 \cdot \pi^2} \cdot h_1 \cdot [\ln(\pi \cdot \tau \cdot f_h) + 1.04]$	$\frac{6}{\pi^2} \cdot h_1 \cdot [\ln(\pi \cdot \tau \cdot f_h) + 0.96]$
$f_0^2 \cdot h_2 \cdot f^0$	$\frac{1}{2 \cdot \pi^2} \cdot h_2 \cdot f_h$	$\frac{3}{2 \cdot \pi^2} \cdot h_2 \cdot f_h$	$\frac{5}{\pi^2} \cdot h_2 \cdot f_h$

A single-sided (positive) PSD is assumed, which requires integration form 0 to infinity. It can clearly be seen that, although it has an impact on the convergence, the dependence on τ does not change as a function of the order of the structure function [92, 164]

as it was previously analyzed to the outcome of structure functions of a deterministic function. Assume the following deterministic phase time error:

$$x(t) = \sum_{k=0}^{M} \frac{A_k}{k!} \cdot t^k \tag{C.37}$$

where M denotes the maximum polynomial drift order. Since the N-th increment of this function corresponds to the N-th derivative (or at least its numerical approximation), the outcome of the increment is equal to zero. This means that the drift on the time-domain measurement of the phase error can completely be suppressed by choosing a high order of the structure function. If $N = M$ the outcome will be independent of t and be equal to:

$$\Delta^M x(t) = \tau^N \cdot A_N = \sqrt{D_x^M(\tau)} \tag{C.38}$$

which only depends on the observation time τ. The τ-dependency of this deterministic increment looks very similar to the previously obtained values of the stochastic process in Table C.2. Can a distinction be made between these types of processes? Table C.3 compares the τ-dependency of the structure functions for different orders of polynomial drift. This shows that the dependency to τ of the structure functions is always different for deterministic and stochastic processes. This allows to determine unambiguously the highest polynomial phase drift order. By subtracting the resulting orders, it is possible to determine the lower-order terms and even the complete polynomial. In this way, noise measurements can completely be detrended and analyzed in detail.

In [164] an algorithm to determine the highest-order of frequency drift and for the presence of (higher order) Flicker-noise:

- [Initialize] Set order $i = 1$

Table C.3 τ-dependency of structure functions of deterministic and stochastic processes

Deterministic		Stochastic	
M	$\frac{\sqrt{D_x^M(\tau)}}{\tau}$	α_m	$\frac{\sqrt{D_x^M(\tau)}}{\tau}$
2	$A_2 \cdot \tau$	-2	$\sim\tau^{1/2}$
3	$A_3 \cdot \tau^2$	-4	$\sim\tau^{3/2}$
4	$A_4 \cdot \tau^3$	-6	$\sim\tau^{5/2}$

In the left column, the maximum order of the polynomial is given. The second column shows the outcome of the structure function of order $N = M$. The third column shows the lowest α, α_m for which the stochastic process $S_y(f) = h_\alpha \cdot f^\alpha$ has a bounded structure function of order M. The last column shows the outcome of the normalized structure function for the particular α_m power-law in $S_y(f)$ [92, 164]

- [Test for stationarity] Calculate $\hat{D}_{\phi}^{(i)}(\tau)$ and check whether it is stationary (time-independent), using several samples. If not, increase i by 1 and try again. If yes, set order of frequency drift to $i-1$ and go further.
- [Test for boundedness] If $\hat{D}_{\phi}^{(i)}(\tau)$ is not bounded; increase i by 1 and try again. If yes, set $M=i$ and go further.
- [End] Calculate $S_{\phi}(\omega)$ from $\hat{D}_{\phi}^{(i)}(l\tau)$, $l=1, ..., l_{max}$.

The last step, however, appears to be a difficult task; in [164] two approaches are demonstrated. One can also use $\hat{D}_{\phi}^{(i)}(l\tau)$, $l=1, ..., l_{max}$ to do a curve-fitting using the terms in Table C.2.

Appendix D
Comparison to the State of the Art

This appendix contains four tables containing a comparison of oscillator implementations from literature. The reported specifications of all references are spread over 4 tables, Tables D.1, D.2, D.3 and D.4. The specifications of the implementations which have been discussed in Part II of this work are found at the bottom of every table. Values and references printed in italic, are based on simulations only.

Some of the phase noise FoM values are calculated using (3.63) when only the jitter is reported. Note that this results in an overestimate of the noise spectrum, since this also includes jitter coming from the output circuitry (which is not accumulated in the oscillator).

Table D.1 Comparison to the state of the art

References	Tech. (µm)	f_{tank} (f_{out}) (MHz)	Topology	Voltage (V)	Power (mW)
[178], JSSC	0.35	1,536 (96)	LC harm.	5 (3.3)	31.35
	0.35	1,536 (12)	LC harm.	5 (3.3)	31.35
[177], ISCAS	0.25	900 (25)	LC harm.	3.3	59.4
	0.25	900 (25)	LC harm.	3.3	59.4
[175], FCS	0.13	3,000 (6–133)	LC harm.	3.3	6.6
[281], ISSCC	0.35	9,800	LC harm.	2.2	11.88
	0.35	9,800	LC harm.	2.2	11.88
[252], MWCL	0.18	4,610	LC harm.	1.5	3
	0.18	5,000	LC harm.	1.5	3
[117], MWCL	0.18	5,600	LC harm.	1.2	2.4
[165], EL	0.18	5,470	LC harm.	1.2	5.04
	0.18	5,470	LC harm.	1.2	5.04
[166], EL	0.18	5,500	LC harm.	1.2	3
[77], WAS	0.25	1,800	LC harm.	1.1	0.17
	0.25	1,800	LC harm.	1.1	0.17

(continued)

V. De Smedt et al., *Temperature- and Supply Voltage-Independent Time References for Wireless Sensor Networks*, Analog Circuits and Signal Processing 128,
DOI 10.1007/978-3-319-09003-0

Table D.1 (continued)

References	Tech. (µm)	f_{tank} (f_{out})(MHz)	Topology	Voltage (V)	Power (mW)
[150], MWCL	0.18	2,300	LC harm.	1.5	0.97
	0.18	2,300	LC harm.	1.5	0.97
[148], MWCL	0.18	2,630	LC harm.	0.45	0.43
	0.18	2,645	LC harm.	0.45	0.43
[119], ICECS	0.25	2,400	LC harm.	1.5	0.08
	0.25	2,400	LC harm.	1.5	0.08
[155], JSSC	0.13	5,121	LC Ring	0.5	4.01
	0.13	5,341	LC harm.	0.5	1.01
[234], FCS	0.18	1,700 (1–133)	LC harm.	3.3	23.1 (25 MHz)
[3], FCS	0.18	−(1–133)	LC harm.	3.3	23.43 (25 MHz)
[238], ISSSE	Bip.	0.01–10	LR	–	–
[250, 251], JSSC	0.18	14	RC rel.	1.8	45 µ
	0.18	14	RC rel.	1.8	45 µ
[29], ISSCC	0.13	3.2	IV-C rel.	1.5	38.4 µ
[94], JSSC	0.8	1.5	IV-C ring	5	1.8
[90], ISSCC	65 n	12	IV-C rel.	1.2	90 µ
[192], SBCCI	0.5	12.8	IV-C rel.	3	0.4
[275], SBCCI	0.5	11.6/21.4	IV-C rel.	3	0.4
[195], ISCAS	0.13	2	IV-C rel.	1.8	3 µ
[162], ESSCIRC	0.18	31.25 k	IV-C rel.	1.8	360 n
[254], ICECS	0.18	6.66 k	IV-C rel.	1.5	940 n
	0.18	6.66 k	IV-C rel.	1.5	940 n
[197], ISSCC	65 n	9–30 k	IV-C rel.	1	120 n
	65 n	9–30 k	IV-C rel.	1	120 n
[244], JSSC	0.25	7	Ring	2.4	1.5
[149], VLSI	0.18	10	Ring	1.2	80 µ
[257], ESSCIRC	0.35	2–100	Ring	1.8	0.18 (30 MHz)
	0.35	2–100	Ring	1.8	0.18 (30 MHz)
[225], JSSC	65 n	0.1	MV-C rel.	1.2	41 µ
[227], JSSC	65 n	0.15 (20 Hz)	MV-C rel.	1.2	51 µ
	65 n	0.15 (20 Hz)	MV-C rel.	1.2	51 µ
[71], TCAS-I	0.35	3.3 k	MV-C rel.	1	11 n
[126], JSSC	0.7	1.6	ETF-FLL	5	7.8
T-Wien bridge	65 n	6	RC harm.	1.2	66 µ
	65 n	6	RC harm.	1.2	66 µ
V-Wien bridge	0.13	24	RC harm.	0.9	33 µ
Pulsed oscillator	0.13	48–1,540	Pulsed LC	1.1	46 µ
Inj.-locked 1	0.13	950–1,150	RC harm.	1.0	127 µ
Inj.-locked 2	40 n	23–36	RC harm.	1.0	72 µ

Table D.2 Comparison to the state of the art: noise

References	Jit. (ps)	PN (Δf) (dB) (MHz)	FoM_{PN} (dB)	Tuning (Range) (%/V) (V)	$FoM_{PN,tuned}$ (dB)
[178]	6.78	–	128.6[a]	–	–
	8.96	–	135.2[a]	–	–
[177]	3.927	−114(0.1)	136.4[a]	–	–
	3.927	−143(1)	153.2	–	–
[175]	2	−73.97 (12 k)	152.0[a]	–	–
[281]	–	−93 (0.1)	182.1	1.37 (2)	183.5
	–	−118 (1)	187.1	1.37 (2)	188.5
[252]	–	−120.99 (1)	189.5	3.38 (2.4)	194.8
	–	−120.42 (1)	189.6	3.38 (2.4)	194.9
[117]	–	−119.13 (1)	190.3	8.93 (1.2)	199.8
[165]	–	−102 (0.1)	190.2	–	–
	–	−122.4 (1)	189.7	–	–
[166]	–	−121.3 (1)	191.1	–	–
[77]	–	−126.2 (1)	199.0	–	–
	–	−144.4 (8)	199.1	–	–
[150]	–	−111 (1)	179.2	8.99 (1.5)	188.7
	–	−133 (1, locked)	200.4	–	–
[148]	–	−105.9 (0.4)	185.9	7.30 (1.05)	194.6
	–	−106.4 (0.4)	184.8	7.30 (1.05)	193.4
[119]	–	−73.62 (0.6)	156.6	5.19 (1.5)	163.8
	–	−82.44 (1)	161.0	5.19 (1.5)	168.2
[155]	–	−121.6 (0.6)	194.2	–	–
	–	−116.1 (0.6)	195.1	–	–
[234]	2.8 (100 MHz)	−82 (0.01)	148.4	–	–
[3]	2 (125 MHz)	−82 (0.01)	150.2	–	–
[238]	–	–	–	–	–
[250, 251]	–	– (4, 100 k)	146.0	–	–
	–	– (10 k)	148.0	–	–
[29]	455	–	135.9[a]	–	–
[94]	65	−102 (10 k)	150.7	–	–
[90]	–	−82.125 (10 k)	162.0	–	–
[192]	<0.1 %	–	–	–	–
[275]	<0.1 %	–	–	–	–
[195]	–	–	–	–	–
[162]	–	–	–	–	–
[254]	–	−50 (10 Hz)	136.7	–	–
	–	−89 (1 kHz)	137.4	–	–
[197]	–	–	–	–	–
	–	–	–	–	–
[244]	–	–	–	–	–

(continued)

Table D.2 (continued)

References	Jit. (ps)	PN (Δf) (dB) (MHz)	FoM_{PN} (dB)	Tuning (Range) (%/V) (V)	$FoM_{PN,tuned}$ (dB)
[149]	–	–	–	–	–
[257]	–	−32 (1 k)	129.0	–	–
	–	−96 (1)	133.0	–	–
[225]	52 n	–	109.6[a]	–	–
[227]	–	–	–	–	–
	–	–	–	–	–
[71]	–	–	–	–	–
[126]	320	–	119.2[a]	–	–
T-Wien bridge	127[a]	−73.7 (10 k)	141.1	–	–
	127[a]	−94.6 (100 k)	142.0	–	–
V-Wien bridge	–	–	–	–	–
Pulsed oscillator	49.6	–	142.7[a]	–	–
Inj.-locked 1	–	–	–	–	–
Inj.-locked 2	–	–	–	–	–

[a] Calculation based on the reported jitter/phase noise value, using (3.63)

Table D.3 Comparison to the state of the art: voltage dependency

References	V-range (V)	Rel. V-range (%)	Sensitivity (ppm/V)	Sensitivity (ppm/%)	Remarks
[178]	4.5–5.5	20.0	38	1.85	Bandgap reg.
	4.5–5.5	20.0	38	1.85	Bandgap reg.
[177]	2.97–3.63	20.0	91	3.00	Open loop, bandgap
	2.97–3.63	20.0	91	3.00	Open loop, bandgap
[175]	3.0–3.6	18.2	3.3[a]	0.11[a]	Bandgap reg.
[281]	–	–	–	–	–
	–	–	–	–	–
[252]	–	–	–	–	–
	–	–	–	–	–
[117]	–	–	–	–	–
[165]	–	–	–	–	–
	–	–	–	–	–
[166]	–	–	–	–	–
[77]	–	–	–	–	–
	–	–	–	–	–
[150]	–	–	–	–	–
	–	–	–	–	–

(continued)

Table D.3 (continued)

References	V-range (V)	Rel. V-range (%)	Sensitivity (ppm/V)	Sensitivity (ppm/%)	Remarks
[148]	–	–	–	–	–
	–	–	–	–	–
[119]	–	–	–	–	–
	–	–	–	–	–
[155]	–	–	–	–	–
	–	–	–	–	–
[234]	3–3.6	18.2	100	3.3	T-Null
[3]	3–3.6	18.2	167	5.5	T-Null
[238]	–	–	–	–	–
[250, 251]	1.7–1.9	11.1	16,000	288	V-avg. feedback
	1.7–1.9	11.1	16,000	288	V-avg. feedback
[29]	1.4–1.6	13.3	40,000	600	Offset canceling
[94]	–	–	–	–	–
[90]	–	–	–	–	–
[192]	2.5–5.5	75.0	5,500	222	Bandgap reg.
[275]	3.0–5.5	58.8	6,400	272	Bandgap reg.
[195]	1.8–2.5	32.6	2.8e5	6140	Self-biasing
[162]	–	–	50,000	900	Self-biasing
[254]	0.8–1.8	76.9	9,800	127	PN-resistor
	0.8–1.8	76.9	9,800	127	PN-resistor
[197]	1.5–3.3	75.0	10,000	240	Bandgap ref.
	1.5–3.3	75.0	10,000	240	Bandgap ref.
[244]	2.4–2.75	13.6	17,700	456	Bandgap reg.
[149]	1.2–3.0	85.7	556	11.7	Bandgap reg.
[257]	1.8–3.0	50.0	40,000	960	Ext. voltage,
	1.8–3.0	50.0	40,000	960	PN-resistor
[225]	1.12–1.4	22.2	7,140	90	Ext. PTAT
[227]	–	–	–	–	–
	–	–	–	–	–
[71]	1.0–2.5	85.7	35,000	613	MOS PTAT
[126]	–	–	–	–	–
T-Wien bridge	1.08–1.32	20	*25,000*	*300*	PN-resistor
	1.08–1.32	20	*25,000*	*300*	PN-resistor
V-Wien bridge	0.4–1.4	111	104	0.94	Dual. reg.
Pulsed oscillator	0.6–1.6	91	74	0.81	(External) Self-biasing
Inj.-locked 1	0.7–1.6	78	0	0	Inj. locked
Inj.-locked 2	0.7–1.5	73	0	0	AM-Inj. locked

[a] Estimated value from total reported frequency deviation

Table D.4 Comparison to the state of the art: temperature dependency

References	T-Range (°C)	Sensitivity (ppm/°C)	Trimming/ Calibration	Area (core) (mm^2)	Abs. accuracy (ppm)
[178]	−10–85	12.3 (8.1)	Digital	(0.22)	±100
	−10–85	12.3 (8.1)	Digital	(0.22)	±100
[177]	−5–75	5.25 (3.8)	Digital	–	±152[a]
	−5–75	5.25 (3.8)	Digital	–	±152[a]
[175]	0–70	2.3	Digital	0.81	±277[a]
[281]	–	–	–	0.40 (0.14)	–
	–	–	–	0.40 (0.14)	–
[252]	–	–	–	0.41	–
	–	–	–	0.41	–
[117]	–	–	–	0.60	–
[165]	–	–	–	–	–
	–	–	–	–	–
[166]	–	–	–	0.30	–
[77]	–	–	–	–	–
	–	–	–	–	–
[150]	–	–	–	0.79	–
	–	–	–	0.79	–
[148]	–	–	–	2.00	–
	–	–	–	2.00	–
[119]	–	–	–	0.59	–
	–	–	–	0.59	–
[155]	–	–	–	0.73	–
	–	–	–	0.73	–
[234]	−40–85	3.5 (1.6)	Dig.ext.wobble	–	±40
[3]	0–70	1 (0.29)	Dig.ext.wobble	–	±50
[238]	–	–	–	–	–
[250, 251]	−40–125	150 (91)	No	(0.04)	*±4,000*
	−40–125	150 (91)	No	(0.04)	*±4,000*
[29]	20–60	125	Digital, 1-pt.	(0.073)	±1,500
[94]	–	–	–	(1.17)	–
[90]	–	–	–	(0.03)	–
[192]	−40–125	625 (424)	Digital, 1-pt.	(0.18)	–
[275]	−40–125	303	Digital, 1-pt.	(0.19)	–
[195]	−35–85	417	1-Point	2.9 (0.015)	–

(continued)

Table D.4 (continued)

References	T-Range (°C)	Sensitivity (ppm/°C)	Trimming/ Calibration	Area (core) (mm^2)	Abs. accuracy (ppm)
[162]	−45–80	4,000	1-Point	(0.016)	±155
[254]	−40–120	56.9	No	(0.09)	±8,000
	−40–120	56.9	No	(0.09)	±8,000
[197]	0–90	22.2	No	(0.032)	–
	−40–90	38.5	No	(0.032)	–
[244]	−40–125	315 (60–102)	No	1.6	±22,000
[149]	−20–120	66.7	No	(0.22)	–
[257]	−20–100	90	No	(0.08)	±27,000
	−20– 100	90	No	(0.08)	±27,000
[225]	−40–85	320	1-Point	(0.11)	±37,00
[227]	−55–125	55.6	2-Point	(0.2)	±60,000[b]
	−55–125	300	1-Point	(0.2)	±60,000[b]
[71]	−20–80	500	No	(0.1)	±2*e*5
[126]	−55–125	11.2	1-Point	6.75	±1,000
T-Wien bridge	0–120	86.1 (75)	No	(0.03)	±8,800
	0–120	*33*	No	(0.03)	±8,800
V-Wien bridge	–	1*e*4	No	(0.03)	±4,600
Pulsed oscillator	−40–100	48–1,540	No	2.63	±7,600
Inj.-locked 1	−20–100	950–1,150	No	0.18 (0.0022)	–
Inj.-locked 2	−20–100	23–36	No	0.165 (0.0017)	–

[a] Including all external variations
[b] Uncompensated, before trimming

References

1. Adams, J.: An introduction to IEEE std 802.15.4. In: Aerospace Conference, 2006 IEEE, 8 pp. (2006). doi:10.1109/AERO.2006.1655947
2. Adler, R.: A study of locking phenomena in oscillators. In: Proceedings of the IRE **34**(6), 351–357 (1946). doi:10.1109/JRPROC.1946.229930
3. Ahmed, A., Hanafi, B., Hosny, S., Sinoussi, N., Hamed, A., Samir, M., Essam, M., El-Kholy, A., Weheiba, M., Helmy, A.: A highly stable cmos self-compensated oscillator (sco) based on an lc tank temperature null concept. In: Frequency Control and the European Frequency and Time Forum (FCS), 2011 Joint Conference of the IEEE International, pp. 1–5 (2011). doi:10.1109/FCS.2011.5977850
4. Alford, R.C., Stengel, R.E., Weisman, D.H., Marlin, G.W.: Method of forming a three-dimensional integrated inductor (1999). US Patent 6,008,102
5. Allan, D.: Should the classical variance be used as a basic measure in standards metrology? IEEE Trans. Instrum. Measur. **IM-36**(2), 646–654 (1987). doi:10.1109/TIM.1987.6312761
6. Andreani, P., Sjoland, H.: Tail current noise suppression in rf cmos vcos. IEEE J. Solid-State Circ. **37**(3), 342–348 (2002). doi:10.1109/4.987086
7. Appleton, E., Greaves, W.: XLIII on the solution of the representative differential equation of the triode oscillator. Lond. Edinb. Dublin Philos. Mag. J. Sci. **45**(267), 401–414 (1923)
8. Arden, W.M.: The international technology roadmap for semiconductorsperspectives and challenges for the next 15 years. Curr. Opin. Solid State Mater. Sci. **6**(5), 371–377 (2002)
9. Atalla, M., Tannenbaum, E., Scheibner, E.: Stabilization of silicon surfaces by thermally grown oxides. Bell Syst.Tech. J. **38**, 749–783 (1959)
10. Baghaei-Nejad, M., Mendoza, D., Zou, Z., Radiom, S., Gielen, G., Zheng, L.R., Tenhunen, H.: A remote-powered rfid tag with 10mb/s uwb uplink and −18.5 dbm sensitivity uhf downlink in 0.18 μm cmos. In: Solid-State Circuits Conference—Digest of Technical Papers, 2009. ISSCC 2009. IEEE International, pp. 198–199,199a (2009). doi:10.1109/ISSCC.2009.4977376
11. Ball, P.: Nature news - precise atomic clock may redefine time. http://www.nature.com/news/precise-atomic-clock-may-redefine-time-1.13363 (2013)
12. Bastos, J., Steyaert, M., Graindourze, B., Sansen, W.: Matching of mos transistors with different layout styles. In: ICMTS 1996. Proceedings. IEEE International Conference on Microelectronic Test Structures, pp. 17–18 (1996). doi:10.1109/ICMTS.1996.535615
13. Batur, O., Akdag, E., Akkurt, H., Oncu, A., Koca, M., Dundar, G.: An ultra low-power dual-band ir-uwb transmitter in 130-nm cmos. IEEE Trans. Circ. Syst. II: Express Briefs **59**(11), 701–705 (2012). doi:10.1109/TCSII.2012.2218474
14. Behzad, A., Shi, Z.M., Anand, S., Lin, L., Carter, K., Kappes, M., Lin, T.H., Nguyen, T., Yuan, D., Wu, S., Wong, Y.C., Fong, V., Rofougaran, A.: A 5-GHz direct-conversion CMOS transceiver utilizing automatic frequency control for the IEEE 802.11 a wireless LAN standard. IEEE J. Solid State Circ. **38**(12), 2209–2220 (2003). doi:10.1109/JSSC.2003.819085
15. Bellis, M.: History of electromagnetism—innovations using magnetic fields. http://inventors.about.com/od/estartinventions/a/Electromagnets.htm (2013)

V. De Smedt et al., *Temperature- and Supply Voltage-Independent Time References for Wireless Sensor Networks*, Analog Circuits and Signal Processing 128,
DOI 10.1007/978-3-319-09003-0

16. Bellis, M.: The history of the integrated circuit aka microchip. http://inventors.about.com/od/istartinventions/a/intergrated_circuit.htm (2013)
17. Belmans, R.: Elektrische energie-Dl 2. Garant (2002)
18. Beow Yew Tan, P., Victor Kordesch, A., Sidek, O.: Analysis of Poly Resistor Mismatch. ICSE'06. IEEE International Conference on Semiconductor Electronics, 2006, pp. 1028–1029 (2006). doi:10.1109/SMELEC.2006.380795
19. Bracke, W., Merken, P., Puers, R., Van Hoof, C.: Ultra-low-power interface chip for autonomous capacitive sensor systems. IEEE Trans. Circ. Syst. I: Regul. Pap. **54**(1), 130–140 (2007). doi:10.1109/TCSI.2006.887978
20. Brandt, L.: Rückblick auf die deutsche funkmeßtechnik. In: Forschen und Gestalten. Springer, Berlin, pp. 53–79 (1962)
21. Bucher, M., Lallement, C., Enz, C., Krummenacher, F.: Accurate mos modelling for analog circuit simulation using the ekv model. In: 1996 IEEE International Symposium on Circuits and Systems, 1996. ISCAS'96, Connecting the World, vol. 4, pp. 703–706 (1996). doi:10.1109/ISCAS.1996.542121
22. Budak, A., Nay, K.: Operational amplifier circuits for the Wien-bridge oscillator. IEEE Trans. Circ. Syst. **28**(9), 930–934 (1981)
23. Buisson, O.R.D., Morin, G.: Mosfet matching in a deep submicron technology. In: Solid State Device Research Conference, 1996. ESSDERC'96. Proceedings of the 26th European, pp. 731–734 (1996)
24. Canada, R.W.: Boost in rfid from gigantic growth of internet of things (iot) and internet of objects (ioo). http://www.rfidworld.ca/boost-in-rfid-from-gigantic-growth-of-internet-of-things-iot-and-internet-of-objects-ioo/1691 (2013)
25. Carnes, J., Vytyaz, I., Hanumolu, P., Mayaram, K., Moon, U.K.: Design and analysis of noise tolerant ring oscillators using maneatis delay cells. In: 14th IEEE International Conference on Electronics, Circuits and Systems, 2007. ICECS 2007, pp. 494–497 (2007). doi:10.1109/ICECS.2007.4511037
26. Chee, Y.H., Niknejad, A., Rabaey, J.: An ultra-low-power injection locked transmitter for wireless sensor networks. IEEE J. Solid State Circ. **41**(8), 1740–1748 (2006). doi:10.1109/JSSC.2006.877254
27. Cheng, Y.: The influence and modeling of process variation and device mismatch for analog/rf circuit design. In: Proceedings of the Fourth IEEE International Caracas Conference on Devices, Circuits and Systems, 2002, pp. D046-1–D046-8 (2002). doi:10.1109/ICCDCS.2002.1004068
28. Cho, H., Bae, J., Yoo, H.J.: A 37.5 μw body channel communication wake-up receiver with injection-locking ring oscillator for wireless body area network. In: IEEE Trans. Circ. Syst. I: Regul. Pap. **60**(5), 1200–1208 (2013). doi:10.1109/TCSI.2013.2249173
29. Choe, K., Bernal, O., Nuttman, D., Je, M.: A precision relaxation oscillator with a self-clocked offset-cancellation scheme for implantable biomedical socs. In: Solid-State Circuits Conference—Digest of Technical Papers, 2009. ISSCC 2009. IEEE International, pp. 402–403, 403a (2009). doi:10.1109/ISSCC.2009.4977478
30. Choi, Y.S., Yoon, J.B.: Experimental analysis of the effect of metal thickness on the quality factor in integrated spiral inductors for RF ICS. IEEE Electron Device Lett. **25**(2), 76–79 (2004). doi:10.1109/LED.2003.822652
31. Chuang, H.M., Thei, K.B., Tsai, S.F., Liu, W.C.: Temperature-dependent characteristics of polysilicon and diffused resistors. IEEE Trans. Electron Devices **50**(5), 1413–1415 (2003). doi:10.1109/TED.2003.813472
32. Clarke, K.: Wien bridge oscillator design. Proc. IRE **41**(2), 246–249 (1953). doi:10.1109/JRPROC.1953.274213
33. Compaq, Hewlett-Packard, Intel, Lucent, Microsoft, NEC, Philips: Universal serial bus specification, rev.2.0, apr. 27, 2000. Sec 7(1) (2000)
34. Couch, L.W., Kulkarni, M., Acharya, U.S.: Digital and analog communication systems, vol. 6. Prentice Hall, Upper Saddle River (1997)

35. Couch, L.W.: A study of a driven oscillator with fm feedback by use of a phase-lock-loop model. IEEE Trans. Microwave Theor. Techniques **19**(4), 357–366 (1971). doi:10.1109/TMTT.1971.1127520
36. Courant, R., Hilbert, D.: Methods of Mathematical Physics, vol. 1. Wiley, London (2008)
37. Craninckx, J., Steyaert, M.: A 1.8-GHz CMOS low-phase-noise voltage-controlled oscillator with prescaler. IEEE J. Solid-State Circ. **30**(12), 1474–1482 (1995). doi:10.1109/4.482195
38. Craninckx, J., Steyaert, M.: Low-noise voltage-controlled oscillators using enhanced LC-tanks. IEEE Trans. Circ. Syst. II Analog Digital Signal Process. **42**(12), 794–804 (1995). doi:10.1109/82.476177
39. Crepaldi, M., Li, C., Fernandes, J., Kinget, P.: An ultra-wideband impulse-radio transceiver chipset using synchronized-OOK modulation. IEEE J. Solid-State Circ. **46**(10), 2284–2299 (2011). doi:10.1109/JSSC.2011.2161214
40. Cunha, A., Schneider, M., Galup-Montoro, C.: An MOS transistor model for analog circuit design. IEEE J. Solid-State Circ. **33**(10), 1510–1519 (1998). doi:10.1109/4.720397
41. Cutler, L., Searle, C.: Some aspects of the theory and measurement of frequency fluctuations in frequency standards. Proc. IEEE **54**(2), 136–154 (1966). doi:10.1109/PROC.1966.4627
42. D'Angelo, K.P., Wrathall, R.S.: Compact low dropout voltage regulator using enhancement and depletion mode MOS transistors (1999)
43. Danneels, H.: CMOS, time-based, digital-oriented, integrated sensor interfaces (CMOS, tijdsgebaseerde, digitaal georienteerde, geintegreerde sensor interfaces) (2013)
44. Danneels, H., Coddens, K., Gielen, G.: An enhanced, highly linear, fully-differential PLL-based sensor interface. Procedia Engineering, vol 46. (2011)
45. Danneels, H., Coddens, K., Gielen, G.: A fully-digital, 0.3v, 270 nw capacitive sensor interface without external references. In: 2011 Proceedings of the ESSCIRC (ESSCIRC), pp. 287–290 (2011). doi:10.1109/ESSCIRC.2011.6044963
46. Danneels, H., De Smedt, V., De Roover, C., Radiom, S., Van Helleputte, N., Walravens, C., Li, Z., Steyaert, M., Verhelst, M., Dehaene, W., et al.: An ultra-low-power, batteryless microsystem for wireless sensor networks. Procedia Eng. **47**, 1406–1409 (2012)
47. Darabi, H., Abidi, A.: Noise in rf-cmos mixers: a simple physical model. IEEE J. Solid State Circ. **35**(1), 15–25 (2000). doi:10.1109/4.818916
48. De Muer, B., Borremans, M., Steyaert, M., Li Puma, G.: A 2-GHz low-phase-noise integrated lc-vco set with flicker-noise upconversion minimization. IEEE J. Solid State Circ. **35**(7), 1034–1038 (2000). doi:10.1109/4.848213
49. De Muer, B., Itoh, N., Borremans, M., Steyaert, M.: A 1.8 GHz highly-tunable low-phase-noise CMOS VCO. In: Proceedings of the IEEE 2000 Custom Integrated Circuits Conference, 2000. CICC, pp. 585–588 (2000). doi:10.1109/CICC.2000.852736
50. De Roose, F., De Smedt, V., Volkaerts, W., Steyaert, M., Gielen, G., Reynaert, P., Dehaene, W.: Design of a frequency reference based on a PVT-independent transmission line delay. In: IEEE International Symposium on Circuits and Systems, 2014. ISCAS '14, 1996, Accepted for publication. (2014)
51. De Roover, C.: Wireless energy supply and low power circuits for RFID applications (draadloze energievoorziening en laag vermogen schakelingen voor rfid toepassingen). status: published (2011)
52. De Roover, C., Steyaert, M.: A fully integrated wireless power supply for pinless active RFID-devices in 130 nm CMOS. Solid-State Circuits Conference, 2007. ASSCC '07. IEEE Asian pp. 123–126 (2007). doi:10.1109/ASSCC.2007.4425747
53. De Smedt, V., De Wit, P., Vereecken, W., Steyaert, M.: A fully-integrated wienbridge topology for ultra-low-power 86 ppm/°c 65nm CMOS 6 MHz clock reference with amplitude regulation. In: Solid-State Circuits Conference, 2008. ESSCIRC 2008. 34th European, pp. 394–397 (2008). doi:10.1109/ESSCIRC.2008.4681875
54. De Smedt, V., De Wit, P., Vereecken, W., Steyaert, M.: A 66 μw 86 ppm/c fully-integrated 6 mhz wienbridge oscillator with a 172 db phase noise fom. IEEE J. Solid State Circ. JSSC **44**(7), 1990–2001 (2009). doi:10.1109/JSSC.2009.2021914

55. De Smedt, V., Dehaene, W., Gielen, G.: A 0.4–1.4 v 24mhz fully integrated 33 μw, 104ppm/v supply-independent oscillator for rfids. In: Proceedings of ESSCIRC, 2009. ESSCIRC '09. pp. 396–399 (2009). doi:10.1109/ESSCIRC.2009.5325966
56. De Smedt, V., Gielen, G., Dehaene, W.: A 0.6v to 1.6v, 46 μw voltage and temperature independent 48 mhz pulsed lc oscillator for RFID tags. In: Solid State Circuits Conference (A-SSCC), 2011 IEEE Asian, pp. 109–112 (2011). doi:10.1109/ASSCC.2011.6123616
57. De Smedt, V., Gielen, G., Dehaene, W.: A 127 μw exact timing reference for wireless sensor networks based on injection locking. In: Proceedings of the ESSCIRC (ESSCIRC), 2012, pp. 262–264 (2012). doi:10.1109/ESSCIRC.2012.6341335
58. De Smedt, V., Gielen, G., Dehaene, W.: A novel, highly linear, voltage and temperature independent sensor interface using pulse width modulation. Procedia Engineering 47(0), 1215–1218 (2012). http://dx.doi.org/10.1016/j.proeng.2012.09.371. http://www.sciencedirect.com/science/article/pii/S1877705812044347. 26th European Conference on Solid-State Transducers, EUROSENSORS 2012
59. De Smedt, V., Gielen, G., Dehaene, W.: A 40nm-cmos, 18 μw, temperature and supply voltage independent sensor interface for RFID tags. In: Solid-State Circuits Conference (A-SSCC), 2013 IEEE Asian, pp. 113–116 (2013). doi:10.1109/ASSCC.2013.6690995
60. De Smedt, V., Gielen, G., Dehaene, W.: Development of an ultra-low-power injection-locked PSK receiver architecture. IEEE Transactions on Circuits and Systems—TCAS II, Accepted for publication (2014)
61. De Smedt, V., Gielen, G., Dehaene, W.: Impact analysis of deep-submicron CMOS technologies on the voltage- and temperature-independence of a time-domain sensor interface. Analog integrated Circuits and Signal Processing, Minor revisions (2014)
62. De Smedt, V., Gielen, G.G.E., Dehaene, W.: Transient behavior and phase noise performance of pulsed-harmonic oscillators, In: IEEE Transactions on Circuits and Systems I: Regular Papers, vol. 61, no.7, pp.2119–2128 (2014). doi:10.1109/TCSI.2014.2304670
63. De Smedt, V., Steyaert, W., Dehaene, W., Gielen, G.: Wobble-based on-chip calibration circuit for temperature independent oscillators. Electron. Lett. **48**(16), 1000–1001 (2012)
64. De Wit, M.: Temperature independent resistor (1995). US Patent 5,448,103
65. De Wit, P., Gielen, G.: Design for Variability and Reliability of Analog Integrated Circuits in Nanometer CMOS Technology. KU Leuven—PhD (2013)
66. Dehaene, W., Gielen, G., Steyaert, M., Danneels, H., Desmedt, V., De Roover, C., Li, Z., Verhelst, M., Van Helleputtea, N., Radioma, S., Walravens, C., Pleysier, L.: RFID, where are they? In: Proceedings of ESSCIRC, 2009. ESSCIRC '09. pp. 36–43 (2009). doi:10.1109/ESSCIRC.2009.5325928
67. Demir, A.: Phase noise in oscillators: Daes and colored noise sources. In: Proceedings of the 1998 IEEE/ACM International Conference on Computer-Aided Design, pp. 170–177. ACM (1998)
68. Demir, A.: Phase noise and timing jitter in oscillators with colored-noise sources. IEEE Trans. Circ. Syst. I: Fundam. Theory Appl. **49**(12), 1782–1791 (2002). doi:10.1109/TCSI.2002.805707
69. Demir, A., Mehrotra, A., Roychowdhury, J.: Phase noise and timing jitter in oscillators. In: Proceedings of the IEEE 1998 Custom Integrated Circuits Conference, 1998, pp. 45–48. IEEE (1998)
70. Demir, A., Mehrotra, A., Roychowdhury, J.: Phase noise in oscillators: a unifying theory and numerical methods for characterization. IEEE Trans. Circ. Syst. I: Fundam. Theory Appl. **47**(5), 655–674 (2000). doi:10.1109/81.847872
71. Denier, U.: Analysis and design of an ultralow-power cmos relaxation oscillator. IEEE Trans. Circ. Syst. I: Regular Papers **57**(8), 1973–1982 (2010). doi:10.1109/TCSI.2010.2041504
72. Deval, Y., Tomas, J., Begueret, J., Lapuyade, H., Dom, J.: 1-V low-noise 200 MHz relaxation oscillator. Solid-State Circuits Conference, 1997. ESSCIRC '97. Proceedings of the 23rd European pp. 220–223 (1997)
73. Dictionary, C.: Wireless sensor network (2013). http://www.collinsdictionary.com/dictionary/english/wireless-sensor-networking

74. Dictionary, T.F.: Oscillator (2013). http://www.thefreedictionary.com/oscillator
75. Dierickx, B., Simoen, E.: The decrease of random telegraph signalnoise in metal-oxide-semiconductor field-effect transistors when cycled from inversion to accumulation. J. Appl. Phys. **71**(4), 2028–2029 (1992)
76. Djurhuus, T., Krozer, V.: Theory of injection-locked oscillator phase noise. IEEE Trans. Circ. Syst. I Reg. Pap. **58**(2), 312–325 (2011). doi:10.1109/TCSI.2010.2071770
77. Ebrahimzadeh, M.: Design of an ultra low power low phase noise cmos LC oscillator. World Academy of Science (2011)
78. Elrazaz, Z., Sinha, N.: On the selection of the dominant poles of a system to be retained in a low-order model. IEEE Trans. Autom. Control **24**(5), 792–793 (1979). doi:10.1109/TAC.1979.1102141
79. Office of Engineering and Technology, Federal Communications Commission.: Understanding the fcc regulations for low-power, non-licensed transmitters (1993)
80. Enz, C.C., Krummenacher, F., Vittoz, E.A.: An analytical MOS transistor model valid in all regions of operation and dedicated to low-voltage and low-current applications. Analog Integr. Circ. Sig. Process. **8**(1), 83–114 (1995)
81. Erc, E.R.C.: Spinoff company: Mobius microsystems (2013). http://erc-assoc.org/about/erc_data/spinoff-company-mobius-microsystems
82. Ferre-Pikal, E., Vig, J., Camparo, J., Cutler, L., Maleki, L., Riley, W., Stein, S., Thomas, C., Walls, F., White, J.: Draft revision of IEEE std 1139–1988 standard definitions of physical quantities for fundamental, frequency and time metrology-random instabilities. In: Proceedings of the 1997 IEEE International Frequency Control Symposium, 1997, pp. 338–357 (1997) doi:10.1109/FREQ.1997.638567.
83. Filanovsky, I., Allam, A.: Mutual compensation of mobility and threshold voltage temperature effects with applications in cmos circuits. IEEE Trans. Circ. Syst. I Fundame. Theory Appl. **48**(7), 876–884 (2001). doi:10.1109/81.933328
84. Fraedrich, K.: Estimating weather and climate predictability on attractors. J. Atmos. Sci. **44**(4), 722–728 (1987)
85. Frishman, F.: On the Arithmetic Means and Variances of Products and Ratios of Random Variables. Springer, Berlin (1975)
86. Fuhring, J.: An early coherer radio receiver (2012). http://www.geojohn.org/Radios/MyRadios/Coherer/Coherer.html
87. Galindo, F.J., Palacio, J.: Estimating the instabilities of n correlated clocks. Tech. rep, DTIC Document (1999)
88. Gambini, S., Pletcher, N., Rabaey, J.M.: Sensitivity analysis for am detectors. EECS Department, University of California, Berkeley, Tech. Rep. UCB/EECS-2008-31 (2008)
89. Gangasani, G., Kinget, P.: A time-domain model for predicting the injection locking bandwidth of nonharmonic oscillators. IEEE Trans. Circ. Syst. II: Exp. Briefs **53**(10), 1035–1038 (2006). doi:10.1109/TCSII.2006.882239
90. Geraedts, P., Van Tuijl, E., Klumperink, E., Wienk, G., Nauta, B.: A 90 μw 12 mhz relaxation oscillator with a −162 db fom. In: IEEE International Solid-State Circuits Conference, 2008. ISSCC 2008. Digest of Technical Papers, pp. 348–618 (2008). doi:10.1109/ISSCC.2008.4523200
91. Geraedts, P.F., Tuijl, E.A., Klumperink, E.A., Wienk, G.J., Nauta, B.: Towards minimum achievable phase noise of relaxation oscillators. International Journal of Circuit Theory and Applications (2012)
92. Gierkink, S.L.J.: Control linearity and jitter of relaxation oscillators. Universiteit Twente (1999)
93. Gierkink, S.L.J., Klumperink, E., van der Wel, A., Hoogzaad, G., Van Tuijl, E., Nauta, B.: Intrinsic 1/f device noise reduction and its effect on phase noise in cmos ring oscillators. IEEE J. Solid State Circ. **34**(7), 1022–1025 (1999). doi:10.1109/4.772418
94. Gierkink, S.L.J., van Tuijl, E.: A coupled sawtooth oscillator combining low jitter with high control linearity. IEEE J. Solid State Circ. **37**(6), 702–710 (2002). doi:10.1109/JSSC.2002.1004574

95. Goebel, G.: The british invention of radar (2011). http://www.vectorsite.net/ttwiz_01.html
96. Gonzalez, R., Gordon, B.M., Horowitz, M.A.: Supply and threshold voltage scaling for low power CMOS. IEEE J. Solid-State Circ. **32**(8), 1210–1216 (1997)
97. Grey, P.R., Meyer, R.G.: Analysis and Design of Analog Integrated Circuits. Wiley, New York (1993)
98. Groszkowski, J.: The interdependence of frequency variation and harmonic content, and the problem of constant-frequency oscillators. Proc. Insti. Radio Eng. **21**(7), 958–981 (1933). doi:10.1109/JRPROC.1933.227821
99. Ha, H., Suh, Y., Lee, S.K., Park, H.J., Sim, J.Y.: A 0.5v, 11.3-μw, 1-ks/s resistive sensor interface circuit with correlated double sampling. In: Custom Integrated Circuits Conference (CICC), 2012 IEEE, pp. 1–4 (2012). doi:10.1109/CICC.2012.6330702
100. Hajimiri, A., Lee, T.: Corrections to "a general theory of phase noise in electrical oscillators". IEEE J. Solid State Circ. 33(6), 928–928 (1998). doi:10.1109/4.678662
101. Hajimiri, A., Lee, T.: A general theory of phase noise in electrical oscillators. IEEE J. Solid State Circ. **33**(2), 179–194 (1998). doi:10.1109/4.658619
102. Hajimiri, A., Lee, T.: Design issues in cmos differential LC oscillators. IEEE J. Solid State Circ. **34**(5), 717–724 (1999). doi:10.1109/4.760384
103. Hajimiri, A., Lee, T.H.: Phase noise in CMOS differential LC oscillators. In: 1998 Symposium on VLSI Circuits, 1998. Digest of Technical Papers. pp. 48–51. IEEE (1998)
104. Hajimiri, A., Limotyrakis, S., Lee, T.: Jitter and phase noise in ring oscillators. IEEE J. Solid State Circ. **34**(6), 790–804 (1999). doi:10.1109/4.766813
105. Han, J., Nguyen, C.: On the development of a compact sub-nanosecond tunable monocycle pulse transmitter for UWB applications. IEEE Trans. Microwave Theory Tech. **54**(1), 285–293 (2006). doi:10.1109/TMTT.2005.860299
106. Hanson, S., Zhai, B., Bernstein, K., Blaauw, D., Bryant, A., Chang, L., Das, K.K., Haensch, W., Nowak, E.J., Sylvester, D.M.: Ultralow-voltage, minimum-energy CMOS. IBM J. Res. Dev. **50**(4/5), 469–490 (2006). http://dl.acm.org/citation.cfm?id=1167704.1167714
107. Harris, D.: Lecture 21: Scaling and economics (2004). http://www.cmosvlsi.com/lect21.pdf
108. Hashemi, S., Ghafoorifard, H., Abdipour, A.: Amplitude noise of electrical oscillators based on the LTV model. Electron. Electr. Eng. **18**(8), 31–36 (2012)
109. Helmy, A., Sinoussi, N., Elkholy, A., Essam, M., Hassanein, A., Ahmed, A.: A monolithic CMOS self-compensated LC oscillator across temperature. In: Frequency References, Power Management for SoC, and Smart Wireless Interfaces, pp. 3–22. Springer, Berlin (2014)
110. Herzel, F., Razavi, B.: A study of oscillator jitter due to supply and substrate noise. Circuits and Systems II: Analog and Digital Signal Processing, IEEE Transactions on 46(1), 56–62 (1999). doi:10.1109/82.749085.
111. Hocquet, C., Kamel, D., Regazzoni, F., Legat, J.D., Flandre, D., Bol, D., Standaert, F.X.: Harvesting the potential of nano-CMOS for lightweight cryptography: an ultra-low-voltage 65 nm AES coprocessor for passive RFID tags. J. Cryptographic Eng. **1**(1), 79–86 (2011)
112. Hsiao, K.J.: A 1.89nw/0.15v self-charged XO for real-time clock generation. In: Solid-State Circuits Conference, 2014. ISSCC 2014. Digest of Technical Papers. IEEE International, pp. 298–299 (2014)
113. Huang, X., Ba, A., Harpe, P., Dolmans, G., de Groot, H., Long, J.: A 915mhz 120 μw-rx/900 μw-tx envelope-detection transceiver with 20db in-band interference tolerance. In: 2012 IEEE International Solid-State Circuits Conference Digest of Technical Papers (ISSCC), pp. 454–456 (2012). doi:10.1109/ISSCC.2012.6177088
114. Irwin, J.D., Nelms, R.M.: Basic Engineering Circuit Analysis. Wiley, New York (2008)
115. Iwai, H.: CMOS downsizing toward sub-10 nm. Solid-State Electron. **48**(4), 497–503 (2004)
116. Jana, P., Nandi, R.: Single current conveyor tunable sinewave RC oscillator. Electron. Lett. **20**(1), 44–45 (1984). doi:10.1049/el:19840031
117. Jang, S.L., Liu, C.C., Wu, C.Y., Juang, M.H.: A 5.6 GHz low power balanced vco in 0.18 μm CMOS. Microwave Wireless Compon. Lett. IEEE **19**(4), 233–235 (2009). doi:10.1109/LMWC.2009.2015507

118. Johnson, J.B.: Thermal agitation of electricity in conductors. Phys. Rev. **32**, 97–109 (1928). doi:10.1103/PhysRev.32.97.http://link.aps.org/doi/10.1103/PhysRev.32.97
119. Jou, C.F., Cheng, K.H., Hsieh, H.C.: An ultra low power 2.4 GHz CMOS VCO. In: Proceedings of the 2003 10th IEEE International Conference on Electronics, Circuits and Systems, 2003. ICECS 2003, vol. 3, pp. 1098–1100. IEEE (2003)
120. Kaajakari, V.: Theory and analysis of MEMS resonators (2011). http://www.ieee-uffc.org/frequency-control/learning/pdf/Kaajakari-MEMS_Resonators_v2b.pdf
121. Kaertner, F.X.: Analysis of white and f- α noise in oscillators. Int. J. Circ. Theory Appl. **18**(5), 485–519 (1990)
122. Kahng, D.: Electric field controlled semiconductor device (1963)
123. Kalia, S., Elbadry, M., Sadhu, B., Patnaik, S., Qiu, J., Harjani, R.: A simple, unified phase noise model for injection-locked oscillators. In: Radio Frequency Integrated Circuits Symposium (RFIC), 2011 IEEE, pp. 1–4 (2011). doi:10.1109/RFIC.2011.5940707
124. Kamon, M., Tsuk, M.J., White, J.: Fasthenry: a multipole-accelerated 3-d inductance extraction program pp. 678–683 (1993). http://doi.acm.org/10.1145/157485.165090
125. Kashmiri, S., Makinwa, K.A.A.: Measuring the thermal diffusivity of cmos chips. In: Sensors, 2009 IEEE, pp. 45–48 (2009). doi:10.1109/ICSENS.2009.5398125
126. Kashmiri, S., Pertijs, M.A.P., Makinwa, K.A.A.: A thermal-diffusivity-based frequency reference in standard CMOS with an absolute inaccuracy of ± 0.1 % from -55 °C to 125 °C. IEEE J. Solid-State Circ. **45**(12), 2510–2520 (2010). doi:10.1109/JSSC.2010.2076343
127. Kashmiri, S.M., Makinwa, K.A.: Silicon-based frequency references. In: Electrothermal Frequency References in Standard CMOS. Springer, Berlin, pp. 15–44 (2013)
128. Keller, V.: Re-entangling the thermometer: cornelis drebbels description of his self-regulating oven, the regiment of fire, and the early history of temperature (2013). http://blogs.uoregon.edu/verakeller/files/2013/08/Keller-on-Drebbels-Self-regulating-oven-in-nuncius-v4k192.pdf
129. Kilby, J.: Invention of the integrated circuit. IEEE Trans. Electron Dev. **23**(7), 648–654 (1976). doi:10.1109/T-ED.1976.18467
130. Kilby, J.S.: Method of making miniaturized electronic circuits (1966). http://www.freepatentsonline.com/3261081.html
131. Kim, S.J., Lee, Y.G., Yun, S.K., Lee, H.Y.: Realization of high-q inductors using wirebonding technology. In: The First IEEE Asia Pacific Conference on ASICs, 1999. AP-ASIC '99. pp. 13–16 (1999). doi:10.1109/APASIC.1999.824149
132. King Liu, T.J.: Bulk CMOS scaling to the end of the roadmap (2012). http://www.eecs.berkeley.edu/~tking/presentations/KingLiu_2012VLSI-Cshortcourse
133. Kinget, P.: A fully integrated 2.7 v 0.35 /spl mu/m CMOS VCO for 5 GHz wireless applications. In: 1998 IEEE International Solid-State Circuits Conference, 1998. Digest of Technical Papers. pp. 226–227 (1998). doi:10.1109/ISSCC.1998.672446
134. Kinget, P.: Integrated ghz voltage controlled oscillators. In: Analog Circuit Design, pp. 353–381. Springer, Berlin (1999)
135. Klass, F., Amir, C., Das, A., Aingaran, K., Truong, C., Wang, R., Mehta, A., Heald, R., Yee, G.: A new family of semidynamic and dynamic flip-flops with embedded logic for high-performance processors. IEEE J. Solid State Circ. **34**(5), 712–716 (1999). doi:10.1109/4.760383
136. Klimovitch, G.: Near-carrier oscillator spectrum due to flicker and white noise. In: The 2000 IEEE International Symposium on Circuits and Systems, 2000. Proceedings. ISCAS 2000 Geneva. vol. 1, pp. 703–706 (2000). doi:10.1109/ISCAS.2000.857192
137. Klimovitch, G.: A nonlinear theory of near-carrier phase noise in free-running oscillators. In: Proceedings of the 2000 Third IEEE International Caracas Conference on Devices, Circuits and Systems, 2000, pp. T80/1–T80/6 (2000). doi:10.1109/ICCDCS.2000.869882
138. Koutsoyannopoulos, Y., Papananos, Y.: Systematic analysis and modeling of integrated inductors and transformers in RF IC design. IEEE Transactions on Circuits and Systems II: Analog and Digital Signal Processing **47**(8), 699–713 (2000). doi:10.1109/82.861403

139. Ku, Y., Sun, X.: Chaos in van der pol's equation. J. Franklin Inst. **327**(2), 197–207 (1990). doi:10.1016/0016-0032(90)90016-C. http://www.sciencedirect.com/science/article/pii/001600329090016C
140. Kuhn, W., Ibrahim, N.: Analysis of current crowding effects in multiturn spiral inductors. IEEE Trans. Microwave Theory Tech. **49**(1), 31–38 (2001). doi:10.1109/22.899959
141. Kuhn, W., Yanduru, N.: Spiral inductor substrate loss modeling in silicon RF ics. In: Radio and Wireless Conference, 1998. RAWCON 98. 1998 IEEE, pp. 305–308 (1998). doi:10.1109/RAWCON.1998.709197
142. LM555 data sheet
143. Laker, K.R., Sansen, W.M.: Design of Analog Integrated circuits and systems, vol. 1. McGraw-Hill, New York (1994)
144. Lam, C.S.: A review of the recent development of mems and crystal oscillators and their impacts on the frequency control products industry. In: Ultrasonics Symposium, 2008. IUS 2008. IEEE, pp. 694–704 (2008). doi:10.1109/ULTSYM.2008.0167
145. Landt, J.: The history of RFID. IEEE Potentials **24**(4), 8–11 (2005)
146. Lane, W., Wrixon, G.T.: The design of thin-film polysilicon resistors for analog IC applications. IEEE Trans. Electron. Dev. 36(4), 738–744 (1989). doi:10.1109/16.22479
147. Lawes, R.: Future trends in high-resolution lithography. Appl. Surf. Sci. **154**, 519–526 (2000)
148. Lee, H., Mohammadi, S.: A subthreshold low phase noise cmos LC VCO for ultra low power applications. Microwave Wireless Compon. Lett. IEEE **17**(11), 796–798 (2007)
149. Lee, J., Cho, S.: A 10mhz 80 μw 67 ppm/ °C CMOS reference clock oscillator with a temperature compensated feedback loop in 0.18 μm CMOS In: 2009 Symposium on VLSI Circuits, pp. 226–227 (2009)
150. Lee, S.H., Jang, S.L., Chuang, Y.H., Chao, J.J., Lee, J.F., Juang, M.H.: A low power injection locked LC-tank oscillator with current reused topology. Microwave and Wireless Compon. Lett. IEEE **17**(3), 220–222 (2007)
151. Lee, T., Hajimiri, A.: Oscillator phase noise: a tutorial. J. Solid State Circ. IEEE **35**(3), 326–336 (2000). doi:10.1109/4.826814
152. Lee, T.H.: Planar Microwave Engineering: A Practical Guide to Theory, Measurement, and Circuits. Cambridge University Press, Cambridge (2004)
153. Lee, Y.G., Yun, S.K., Lee, H.Y.: Novel high-q bondwire inductor for mmic. In: Electron Devices Meeting, 1998. IEDM '98. Technical Digest., International, pp. 548–551 (1998). doi:10.1109/IEDM.1998.746418
154. Leeson, D.: A simple model of feedback oscillator noise spectrum. Proc. IEEE **54**(2), 329–330 (1966). doi:10.1109/PROC.1966.4682
155. Li, G., Afshari, E.: A low-phase-noise multi-phase oscillator based on left-handed LC-ring. IEEE J. Solid-State Circ. **45**(9), 1822–1833 (2010). doi:10.1109/JSSC.2010.2054591
156. Li, Z.: System-Level Exploration for Ultra-Low-Power Wireless Sensor Networks. Status: published (2011)
157. Li, Z., Dehaene, W., Gielen, G.: A 3-tier UWB-based indoor localization scheme for ultra-low-power sensor nodes. In: IEEE International Conference on Signal Processing and Communications, 2007. ICSPC 2007, pp. 995–998 (2007). doi:10.1109/ICSPC.2007.4728489
158. Li, Z., Dehaene, W., Gielen, G.: A 3-tier uwb-based indoor localization system for ultra-low-power sensor networks. IEEE Trans. Wireless Commun. **8**(6), 2813–2818 (2009). doi:10.1109/TWC.2009.080602
159. Libelium: Libelium case studies, 50 sensor applications for a smarter world (2013). URL http://www.libelium.com/case-studies/,http://www.libelium.com/top_50_iot_sensor_applications_ranking/
160. Lilienfeld, J.S.E.: Method and apparatus for controlling electric currents (1930). US Patent 1,745,175
161. Lilienfeld, J.S.E.: Device for controlling electric current (1933). US Patent 1,900,018
162. Lim, J., Lee, K., Cho, K.: Ultra low power RC oscillator for system wake-up using highly precise auto-calibration technique. In: 2010 Proceedings of the ESSCIRC, pp. 274–277 (2010). doi:10.1109/ESSCIRC.2010.5619876

163. Lin, J., Yeh, T., Lee, C., Chen, C., Tsay, J., Chen, S., Hsu, H., Chen, C., Huang, C., Chiang, J., Chang, A., Chang, R., Chang, C., Wang, S., Wu, C., Lin, C., Chu, Y., Chen, S., Hsu, C., Liou, R., Wong, S., Tang, D., Sun, J.: State-of-the-art RF/analog foundry technology. In: Proceedings of the 2002 Bipolar/BiCMOS Circuits and Technology Meeting, 2002. pp. 73–79 (2002) doi:10.1109/BIPOL.2002.1042890
164. Lindsey, W., Chie, C.M.: Identification of power-law type oscillator phase noise spectra from measurements. IEEE Trans. Ins. Meas. 27(1), 46–53 (1978). doi:10.1109/TIM.1978.4314616
165. Liu, P., Upadhyaya, P., Jung, J., Heo, D., Kim, J.H., Kim, B.S.: Dynamically switched low-phase-noise LC VCO with harmonic filtering. Electron. Lett. **47**(14), 792–793 (2011)
166. Liu, P., Upadhyaya, P., Jung, J., Heo, D., Kim, J.H., Kim, B.S.: Low phase noise LC VCO with reduced drain current duty cycle. Electron. Lett. **48**(2), 77–78 (2012)
167. Lopez-Villegas, J., Samitier, J., Cane, C., Losantos, P., Bausells, J.: Improvement of the quality factor of rf integrated inductors by layout optimization. IEEE Trans. Microw. Theory Tech. **48**(1), 76–83 (2000). doi:10.1109/22.817474
168. Lu, N.C., Gerzberg, L., Lu, C.Y., Meindl, J.: Modeling and optimization of monolithic polycrystalline silicon resistors. IEEE Trans. Electron Dev. **28**(7), 818–830 (1981). doi:10.1109/T-ED.1981.20437
169. Maffezzoni, P.: Frequency-shift induced by colored noise in nonlinear oscillators. IEEE Trans. Circ. Syst. II Exp. Briefs **54**(10), 887–891 (2007). doi:10.1109/TCSII.2007.902241
170. Makinwa, K.A.A., Snoeij, M.: A CMOS temperature-to-frequency converter with an inaccuracy of less than ± 0.5°C ($3\ \sigma$) from -40°C to 105°C. IEEE J. Solid State Circ **41**(12), 2992–2997 (2006). doi:10.1109/JSSC.2006.884865
171. Maneatis, J.: Low-jitter process-independent DLL and PLL based on self-biased techniques. IEEE J. Solid State Circ. **31**(11), 1723–1732 (1996). doi:10.1109/JSSC.1996.542317
172. Maricau, E., Gielen, G.: Analog IC Reliability in Nanometer CMOS. Springer, Berlin (2013)
173. Martins, N., Lima, L., Pinto, H.: Computing dominant poles of power system transfer functions. IEEE Trans. Power Syst. **11**(1), 162–170 (1996). doi:10.1109/59.486093
174. McCorquodale, M., Carichner, G., O'Day, J., Pernia, S., Kubba, S., Marsman, E., Kuhn, J., Brown, R.: A 25-MHz self-referenced solid-state frequency source suitable for xo-replacement. IEEE Trans. Circ. Syst. I Reg. Pap. **56**(5), 943–956 (2009). doi:10.1109/TCSI.2009.2016133
175. McCorquodale, M., Gupta, B., Armstrong, W.E., Beaudouin, R., Carichner, G., Chaudhari, P., Fayyaz, N., Gaskin, N., Kuhn, J., Linebarger, D., Marsman, E., O'Day, J., Pernia, S., Senderowicz, D.: A silicon die as a frequency source. In: 2010 IEEE International Frequency Control Symposium (FCS), pp. 103–108 (2010). doi:10.1109/FREQ.2010.5556366
176. McCorquodale, M., Gupta, V.: A history of the development of CMOS oscillators: The dark horse in frequency control. In: Frequency Control and the European Frequency and Time Forum (FCS), 2011 Joint Conference of the IEEE International, pp. 1–6 (2011). doi:10.1109/FCS.2011.5977872
177. McCorquodale, M., Pernia, S., Kubba, S., Carichner, G., O'Day, J., Marsman, E., Kuhn, J., Brown, R.: A 25 MHz all-CMOS reference clock generator for xo-replacement in serial wire interfaces. In: IEEE International Symposium on Circuits and Systems, 2008. ISCAS 2008, pp. 2837–2840 (2008). doi:10.1109/ISCAS.2008.4542048
178. McCorquodale, M.S., O'Day, J.D., Pernia, S.M., Carichner, G.A., Kubba, S., Brown, R.B.: A monolithic and self-referenced RF LC clock generator compliant with usb 2.0. IEEE J. Solid State Cir. **42**(2), 385–399 (2007). doi:10.1109/JSSC.2006.883337
179. McCreary, J.: Matching properties, and voltage and temperature dependence of mos capacitors. IEEE J. Solid State Circ. **16**(6), 608–616 (1981). doi:10.1109/JSSC.1981.1051651
180. McNeill, J.: Jitter in ring oscillators. IEEE J. Solid-State Circ. **32**(6), 870–879 (1997). doi:10.1109/4.585289
181. McNeill, J.A., Ricketts, D.S.: The Designer's Guide to Jitter in Ring Oscillators. Springer, Berlin (2009)
182. Mercier, P., Daly, D., Chandrakasan, A.: A 19pj/pulse UWB transmitter with dual capacitively-coupled digital power amplifiers. In: Radio Frequency Integrated Circuits Symposium, 2008. RFIC 2008. IEEE, pp. 47–50 (2008). doi:10.1109/RFIC.2008.4561383

183. Mercier, P.P., Daly, D.C., Chandrakasan, A.P.: An energy-efficient all-digital UWB transmitter employing dual capacitively-coupled pulse-shaping drivers. IEEE J. Solid State Circ. **44**(6), 1679–1688 (2009)
184. Mernyei, F., Darrer, F., Pardoen, M., Sibrai, A.: Reducing the substrate losses of RF integrated inductors. Microwave and Guided Wave Lett. IEEE **8**(9), 300–301 (1998). doi:10.1109/75.720461
185. Mukherjee, J., Roblin, P., Akhtar, S.: An analytic circuit-based model for white and flicker LC oscillators. IEEE Trans. Circ. Syst. I Reg. Pap. **54**(7), 1584–1598 (2007)
186. Namajunas, A., Tamasevicius, A.: Modified wien-bridge oscillator for chaos. Electron. Lett. **31**(5), 335–336 (1995). doi:10.1049/el:19950250
187. Navid, R., Lee, T.H., Dutton, R.W.: Minimum achievable phase noise of RC oscillators. IEEE J. Solid State Circ **40**(3), 630–637 (2005)
188. Nicolson, S., Phang, K.: Improvements in biasing and compensation of CMOS opamps. In: Proceedings of the 2004 International Symposium on Circuits and Systems, 2004. ISCAS '04, vol. 1, pp. I-665–I-6658 (2004). doi:10.1109/ISCAS.2004.1328282
189. Niknejad, A.M.: Injection locking, eecs 242 lecture 26 (2013). http://rfic.eecs.berkeley.edu/~niknejad/ee242/pdf/eecs242_lect26_injectionlocking.pdf
190. NIST, U.N.I.F.S., Technology: Causes of noise sources in a signal source. tf.nist.gov/phase/Properties/twelve.htm
191. Nyquist, H.: Thermal agitation of electric charge in conductors. Phys. Rev. **32**(1), 110–113 (1928)
192. Olmos, A.: A temperature compensated fully trimmable on-chip IC oscillator. Proceedings. 16th Symposium on Integrated Circuits and Systems Design, 2003. SBCCI 2003. pp. 181–186 (2003)
193. Organization: S.A.I.: Serial ATA revision 3.0, June 2, 2009 gold revision (2009)
194. PIC18F2525/2620/4525/4620 data sheet
195. Paavola, M., Laiho, M., Saukoski, M., Halonen, K.: A 3 μW, 2 MHz CMOS frequency reference for capacitive sensor applications. 2006 IEEE International Symposium on Circuits and Systems, 2006. ISCAS 2006. Proceedings. 4 pp. (2006). doi:10.1109/ISCAS.2006.1693602
196. Paciorek, L.J.: Injection locking of oscillators. Proceedings of the IEEE **53**(11), 1723–1727 (1965). doi:10.1109/PROC.1965.4345
197. Paidimarri, A., Griffith, D., Wang, A., Chandrakasan, A., Burra, G.: A 120nw 18.5khz rc oscillator with comparator offset cancellation for $\pm$0.25 temperature stability. In: Solid-State Circuits Conference Digest of Technical Papers (ISSCC), 2013 IEEE International, pp. 184–185 (2013). doi:10.1109/ISSCC.2013.6487692
198. Pelgrom, M., Duinmaijer, A., Welbers, A.: Matching properties of MOS transistors. Solid-State Circuits, IEEE Journal of 24(5), 1433–1439 (1989). doi:10.1109/JSSC.1989.572629
199. Pletcher, N., Gambini, S., Rabaey, J.: A 2ghz 52 μw wake-up receiver with -72dbm sensitivity using uncertain-if architecture. In: Solid-State Circuits Conference, 2008. ISSCC 2008. Digest of Technical Papers. IEEE International, pp. 524–633 (2008). doi:10.1109/ISSCC.2008.4523288
200. Pletcher, N., Gambini, S., Rabaey, J.: A 52 μ w wake-up receiver with $-$72 dbm sensitivity using an uncertain-if architecture. Solid-State Circuits, IEEE Journal of 44(1), 269–280 (2009). doi:10.1109/JSSC.2008.2007438
201. Pletcher, N.M.: Ultra-low power wake-up receivers for wireless sensor networks. ProQuest (2008).
202. Pogge, R.W.: Real-world relativity: The gps navigation system (2009). http://www.astronomy.ohio-state.edu/~pogge/Ast162/Unit5/gps.html
203. Poore, R.: Phase noise and jitter. Agilent EEs of EDA (May 2001)
204. Qian, L., Yeh, W.C.S.: Inductor with cobalt/nickel core for integrated circuit structure with high inductance and high q-factor (2000). US Patent 6,166,422
205. Rabaey, J.: The swarm at the edge of the cloud—a new perspective on wireless. In: VLSI Circuits (VLSIC), 2011 Symposium on, pp. 6–8 (2011)

206. Rabaey, J.M., Chandrakasan, A.P., Nikolic, B.: Digital integrated circuits, vol. 2. Prentice hall Englewood Cliffs (2002)
207. Radiom, S., Baghaei-Nejad, M., Aghdam, K., Vandenbosch, G., Zheng, L.R., Gielen, G.G.E.: Far-field on-chip antennas monolithically integrated in a wireless-powered 5.8-ghz downlink/uwb uplink rfid tag in 0.18-μm standard cmos. Solid-State Circuits, IEEE Journal of 45(9), 1746–1758 (2010). doi:10.1109/JSSC.2010.2055630
208. Radiom, S., Baghaei-Nejad, M., Vandenbosch, G., Zheng, L.R., Gielen, G.: Far-field rf powering system for rfid and implantable devices with monolithically integrated on-chip antenna. In: Radio Frequency Integrated Circuits Symposium (RFIC), 2010 IEEE, pp. 113–116 (2010). doi:10.1109/RFIC.2010.5477377
209. Radiom, S., Enayati, A., Vandenbosch, G., De Raedt, W., Gielen, G.G.E.: Miniaturization of a bow-tie antenna for a pulsed-uwb transceiver in the 300–960 mhz band. In: Antennas and Propagation, 2009. EuCAP 2009. 3rd European Conference on, pp. 3315–3317 (2009)
210. Ramirez, F., Ponton, M., Sancho, S., Suarez, A.: Phase-noise analysis of injection-locked oscillators and analog frequency dividers. Microwave Theory and Techniques, IEEE Transactions on 56(2), 393–407 (2008). doi:10.1109/TMTT.2007.914375
211. Razavi, B.: A study of phase noise in CMOS oscillators. Solid-State Circuits, IEEE Journal of 31(3), 331–343 (1996). doi:10.1109/4.494195
212. Razavi, B.: Design of Analog CMOS Integrated Circuits. McGraw-Hill (2001)
213. Razavi, B.: A study of injection locking and pulling in oscillators. Solid-State Circuits, IEEE Journal of 39(9), 1415–1424 (2004). doi:10.1109/JSSC.2004.831608
214. Reimbold, G., Gentil, P.: White noise of mos transistors operating in weak inversion. Electron Devices, IEEE Transactions on 29(11), 1722–1725 (1982). doi:10.1109/T-ED.1982.21016
215. Risch, L.: Pushing cmos beyond the roadmap. In: Solid-State Circuits Conference, 2005. ESSCIRC 2005. Proceedings of the 31st European, pp. 63–68 (2005). doi:10.1109/ESSCIR.2005.1541558
216. Rommes, J., Sleijpen, G.L.G.: Convergence of the Dominant Pole Algorythm and Reyleigh Quotient Iteration. SIAM Journal on Matrix Analysis and Applications 30(1), 346–363 (2008). doi:10.1137/060671401
217. Rutman, J.: Characterization of phase and frequency instabilities in precision frequency sources: Fifteen years of progress. Proceedings of the IEEE 66(9), 1048–1075 (1978). doi:10.1109/PROC.1978.11080
218. Ryckaert, J., Verhelst, M., Badaroglu, M., D'Amico, S., De Heyn, V., Desset, C., Nuzzo, P., Van Poucke, B., Wambacq, P., Baschirotto, A., Dehaene, W., Van der Plas, G.: A CMOS Ultra-Wideband Receiver for Low Data-Rate Communication. Solid-State Circuits, IEEE Journal of 42(11), 2515–2527 (2007). doi:10.1109/JSSC.2007.907195
219. Sansen, W.: Analog Design Essentials. Springer (2006)
220. Sayed, D., Dessouky, M.: Automatic generation of common-centroid capacitor arrays with arbitrary capacitor ratio. In: Design, Automation and Test in Europe Conference and Exhibition, 2002. Proceedings, pp. 576–580 (2002). doi:10.1109/DATE.2002.998358
221. Schaefer, C.: Rfid in 2011...and beyond (2011). http://www.rfidjournal.net/masterPresentations/rfid_latam2011/np/schaefer_1129_340.pdf
222. Schaller, R.R.: Moore's law: past, present and future. Spectrum, IEEE **34**(6), 52–59 (1997)
223. Schutz, B.: Gravity from the ground up: An Introductory guide to gravity and general relativity. Cambridge University Press (2003)
224. Sebastiano, F., Breems, L., Makinwa, K., Drago, S., Leenaerts, D., Nauta, B.: A low-voltage mobility-based frequency reference for crystal-less ULP radios. Solid-State Circuits Conference, 2008. ESSCIRC 2008. 34th European pp. 306–309 (2008). doi:10.1109/ESSCIRC.2008.4681853
225. Sebastiano, F., Breems, L., Makinwa, K.A.A., Drago, S., Leenaerts, D., Nauta, B.: A low-voltage mobility-based frequency reference for crystal-less ulp radios. Solid-State Circuits, IEEE Journal of 44(7), 2002–2009 (2009). doi:10.1109/JSSC.2009.2020247
226. Sebastiano, F., Breems, L., Makinwa, K.A.A., Drago, S., Leenaerts, D., Nauta, B.: A 1.2-v 10-μw npn-based temperature sensor in 65-nm cmos with an inaccuracy of 0.2 °C (3 σ) from

−70 °C to 125 °C. IEEE J Solid-State Circuits 45(12), 2591–2601 (2010). doi:10.1109/JSSC.2010.2076610
227. Sebastiano, F., Breems, L., Makinwa, K.A.A., Drago, S., Leenaerts, D., Nauta, B.: A 65-nm cmos temperature-compensated mobility-based frequency reference for wireless sensor networks. IEEE J Solid-State Circuits 46(7), 1544–1552 (2011). doi:10.1109/JSSC.2011.2143630
228. Sheng, H., Orlik, P., Haimovich, A., Cimini, L., Zhang, J.: On the spectral and power requirements for ultra-wideband transmission. In: Communications, 2003. ICC '03. IEEE International Conference on, vol. 1, pp. 738–742 (2003). doi:10.1109/ICC.2003.1204271
229. Sheng, W., Xia, B., Emira, A., Xin, C., Valero-Lopez, A., Moon, S.T., Sanchez-Sinencio, E.: A 3-v, 0.35- μm cmos bluetooth receiver ic. Solid-State Circuits, IEEE Journal of 38(1), 30–42 (2003). doi:10.1109/JSSC.2002.806277
230. Shumakher, E., Eisenstein, G.: On the noise properties of injection-locked oscillators. Microwave Theory and Techniques, IEEE Transactions on 52(5), 1523–1537 (2004). doi:10.1109/TMTT.2004.827035
231. Shyu, Y.S., Wu, J.C.: A process and temperature compensated ring oscillator. ASICs, 1999. AP-ASIC '99. The First IEEE Asia Pacific Conference on pp. 283–286 (1999). doi:10.1109/APASIC.1999.824084
232. Siegman, A.E.: Lasers. University Science Books - Mill Valley, CA (1986)
233. Singularity.com: The singularity is near—when humans transcend biology (2014). http://www.singularity.com/charts/page67.html
234. Sinoussi, N., Hamed, A., Essam, M., El-Kholy, A., Hassanein, A., Saeed, M., Helmy, A., Ahmed, A.: A single LC tank self-compensated CMOS oscillator with frequency stability of ±100ppm from −40 °C to 85 °C. In: Frequency Control Symposium (FCS), 2012 IEEE International, pp. 1–5 (2012). doi:10.1109/FCS.2012.6243676
235. Skotnicki, T., Hutchby, J.A., King, T.J., Wong, H.S., Boeuf, F.: The end of CMOS scaling: toward the introduction of new materials and structural changes to improve mosfet performance. Circ. Dev. Mag. IEEE **21**(1), 16–26 (2005)
236. Soltani, N., Yuan, F.: Nonharmonic injection-locked phase-locked loops with applications in remote frequency calibration of passive wireless transponders. IEEE Trans. Circ. Syst. I Reg. Pap. **57**(9), 2381–2393 (2010). doi:10.1109/TCSI.2010.2046228
237. Sparkmuseum: Marconi magnetic detector (2012). http://www.sparkmuseum.com/MAGGIE.HTM
238. Srisuchinwong, B., Trung, N.V.: An integratable current-tunable R-L oscillator. In: 1995 URSI International Symposium on Signals, Systems, and Electronics, 1995. ISSSE '95, Proceedings, pp. 541–544 (1995). doi:10.1109/ISSSE.1995.498051
239. Stanton, T.: Removing the accuracy drift and synchronising the GPS clocks using true relativity and the universal clock (2009). http://www.gsjournal.net/old/science/stanton2.pdf
240. Stork, H.: Economics of CMOS scaling (2005). http://www.etv.tudelft.nl/maxwell/9/1/column.pdf
241. Stork, H.: Economies of CMOS scaling (2005). http://www.nist.gov/pml/div683/conference/upload/Stork_2005.pdf
242. Strogatz, S.: Nonlinear dynamics and chaos: with applications to physics, biology, chemistry, and engineering. Studies in nonlinearity. Sarat Book House (1994). http://books.google.be/books?id=PHmED2xxrE8C
243. Sudevalayam, S., Kulkarni, P.: Energy harvesting sensor nodes: survey and implications. Commun. Surv. Tutorials IEEE **13**(3), 443–461 (2011). doi:10.1109/SURV.2011.060710.00094
244. Sundaresan, K., Allen, P., Ayazi, F.: Process and temperature compensation in a 7-MHz CMOS clock oscillator. IEEE J. Solid State Circ. **41**(2), 433–442 (2006). doi:10.1109/JSSC.2005.863149
245. Svelto, F., Deantoni, S., Castello, R.: A 1.3 GHz low-phase noise fully tunable CMOS LC VCO. IEEE J. Solid State Circ. **35**(3), 356–361 (2000). doi:10.1109/4.826817

246. Székely, V.: Thermal monitoring of microelectronic structures. Microelectron. J. **25**(3), 157–170 (1994)
247. Tanaka, K., Kuramochi, Y., Kurashina, T., Okada, K., Matsuzawa, A.: A 0.026 mm^2 capacitance-to-digital converter for biotelemetry applications using a charge redistribution technique. In: IEEE Asian Solid-State Circuits Conference, 2007. ASSCC '07, pp. 244–247 (2007). doi:10.1109/ASSCC.2007.4425776
248. Tesla, N.: Method of operating arc lamps (1891). US Patent 447,920
249. Tesla, N.: Apparatus for transmitting electrical energy (1914). US Patent 1,119,732
250. Tokunaga, Y., Sakiyama, S., Matsumoto, A., Dosho, S.: An on-chip CMOS relaxation oscillator with power averaging feedback using a reference proportional to supply voltage. IEEE International Solid-State Circuits Conference, 2009. ISSCC 2009. pp. 404–406 (2009)
251. Tokunaga, Y., Sakiyama, S., Matsumoto, A., Dosho, S.: An on-chip CMOS relaxation oscillator with voltage averaging feedback. IEEE J. Solid State Circ. **45**(6), 1150–1158 (2010). doi:10.1109/JSSC.2010.2048732
252. Tsai, M.D., Cho, Y.H., Wang, H.: A 5-GHz low phase noise differential colpitts CMOS VCO. Microw. Wireless Compon. Lett. IEEE **15**(5), 327–329 (2005)
253. Tsividis, Y., McAndrew, C.: Operation and Modeling of the MOS Transistor, vol. 2. Oxford University Press, New York (1999)
254. Tsubaki, K., Hirose, T., Osaki, Y., Shiga, S., Kuroki, N., Numa, M.: A 6.66-khz, 940-nw, 56ppm/°c, fully on-chip PVT variation tolerant CMOS relaxation oscillator. In: 2012 19th IEEE International Conference on Electronics, Circuits and Systems (ICECS), pp. 97–100 (2012). doi:10.1109/ICECS.2012.6463790
255. Tuttlebee, W.: Software-defined radio: facets of a developing technology. Pers. Commun. IEEE 6(2), 38–44 (1999). doi:10.1109/98.760422
256. Ueda, Y., Akamatsu, N.: Chaotically transitional phenomena in the forced negative-resistance oscillator. IEEE Trans. Circ. Syst. **28**(3), 217–224 (1981). doi:10.1109/TCS.1981.1084975
257. Ueno, K., Asai, T., Amemiya, Y.: A 30-MHz, 90-ppm/°c fully-integrated clock reference generator with frequency-locked loop. In: Proceedings of ESSCIRC, 2009. ESSCIRC '09, pp. 392–395 (2009). doi:10.1109/ESSCIRC.2009.5325940
258. USB30: 3.0 specification. Hewlett-Packard Company, Intel Corporation, Microsoft Corporation, NEC Corporation, ST-NXP Wireless, Texas Intruments, rev 1 (2008). www.usb.org
259. Vadasz, L., Grove, A.: Temperature dependence of mos transistor characteristics below saturation. IEEE Trans. Electron Dev. **13**(12), 863–866 (1966). doi:10.1109/T-ED.1966.15860
260. Van Breussegem, T.: Monolithic capacitive CMOS DC–DC converters (monolitische capacitieve CMOS DC–DC convertoren). status: published (2012)
261. Van Helleputte, N.: An ultra-low-power complex analog correlating receiver architecture for UWB impulse radio receivers. status: published (2008)
262. Van Helleputte, N., Verhelst, M., Dehaene, W., Gielen, G.: A reconfigurable, 130 nm CMOS 108 pj/pulse, fully integrated IR-UWB receiver for communication and precise ranging. IEEE J. Solid State Circ. **45**(1), 69–83 (2010)
263. Van Rethy, J., Danneels, H., De Smedt, V., Dehaene, W., Gielen, G.: An energy-efficient BBPLL-based force-balanced wheatstone bridge sensor-to-digital interface in 130 nm CMOS. In: Solid State Circuits Conference (A-SSCC), 2012 IEEE Asian, pp. 41–44 (2012)
264. Van Rethy, J., Danneels, H., De Smedt, V., Dehaene, W., Gielen, G.: Supply-noise-resilient design of a bbpll-based force-balanced wheatstone bridge interface in 130-nm CMOS. IEEE J. Solid State Circ. **48**(11), 2618–2627 (2013). doi:10.1109/JSSC.2013.2274831
265. Van Rethy, J., Danneels, H., De Smedt, V., Gielen, G., Dehaene, W.: A low-power and low-vltage bbpll-based sensor interface in 130 nm CMOS for wireless sensor networks. In: DATE 2013, Grenoble, France, pp. 1431–1435 (2013)
266. Van Rethy, J., Danneels, H., Gielen, G.: Performance analysis of energy-efficient bbpll-based sensor-to-digital converters. IEEE Trans. Circ. Syst. I Reg. Pap. **60**(8), 2130–2138 (2013). doi:10.1109/TCSI.2013.2239097
267. Van Rethy, J., De Smedt, V., Gielen, G., Dehaene, W.: Towards energy-efficient CMOS integrated sensor-to-digital interface circuits. In: AACD '14, Workshop on Advances in Analog Circuit Design, 2014 (2014)

268. Van Rethy, J., Gielen, G.: An energy-efficient capacitance-controlled oscillator-based sensor interface for mems sensors. In: 2013 IEEE Asian Solid State Circuits Conference (A-SSCC), pp. 443–446 (2013)
269. Vanassche, P., Gielen, G., Sansen, W.: On the difference between two widely publicized methods for analyzing oscillator phase behavior. In: Proceedings of the 2002 IEEE/ACM International Conference on Computer-aided Design, pp. 229–233. ACM (2002)
270. Vannerson, E., Smith, K.: Fast amplitude stabilization of an RC oscillator. IEEE J. Solid State Circ. **9**(4), 176–179 (1974)
271. Verhelst, M., Dehaene, W.: System design of an ultra-low power, low data rate, pulsed UWB receiver in the 0–960 MHz band. In: 2005 IEEE International Conference on Communications, 2005. ICC 2005, vol. 4, pp. 2812–2817 (2005). doi:10.1109/ICC.2005.1494864
272. Verhelst, M., Dehaene, W.: A flexible, ultra-low-energy 35 pj/pulse digital back-end for a QAC ir-uwb receiver. IEEE J. Solid State Circ. **43**(7), 1677–1687 (2008). doi:10.1109/JSSC.2008.922711
273. Verhelst, M., Dehaene, W.: Energy Scalable Radio Design: For Pulsed UWB Communication and Ranging. Springer, Berlin (2009)
274. Verhelst, M., Van Helleputte, N., Gielen, G., Dehaene, W.: A reconfigurable, 0.13 um CMOS110pj/pulse, fully integrated IR-UWB receiver for communication and sub-cm ranging. In: Solid-State Circuits Conference—Digest of Technical Papers, 2009. ISSCC 2009. IEEE International, pp. 250–251, 251a (2009). doi:10.1109/ISSCC.2009.4977402
275. Vilas Boas, A., Soldera, J., Olmos, A.: A 1.8 V supply multi-frequency digitally trimmable on-chip IC oscillator with low-voltage detection capability. Integrated Circuits and Systems Design, 2004. SBCCI 2004. pp. 44–48 (2004)
276. Visualisations, C.: The internet of things (2011). http://share.cisco.com/internet-of-things.html
277. Vittoz, E.: Low-power design: ways to approach the limits. In: 1994 IEEE International Solid-State Circuits Conference, 1994. Digest of Technical Papers. 41st ISSCC, pp. 14–18 (1994). doi:10.1109/ISSCC.1994.344744
278. Vittoz, E., Degrauwe, M., Bitz, S.: High-performance crystal oscillator circuits: theory and application. IEEE J. Solid State Circ. **23**(3), 774–783 (1988). doi:10.1109/4.318
279. Volkaerts, W., Marien, B., Danneels, H., De Smedt, V., Reynaert, P., Dehaene, W., Gielen, G.: A 0.5 v–1.4 v supply-independent frequency-based analog-to-digital converter with fast start-up time for wireless sensor networks. In: Proceedings of 2010 IEEE International Symposium on Circuits and Systems (ISCAS), pp. 3096–3099 (2010). doi:10.1109/ISCAS.2010.5537971
280. Walden, R.: Analog-to-digital converter survey and analysis. IEEE J. Sel. Areas Commun. **17**(4), 539–550 (1999). doi:10.1109/49.761034
281. Wang, H.: A 9.8 GHz back-gate tuned VCO in 0.35 μm CMOS. In: Solid-State Circuits Conference, 1999. Digest of Technical Papers. ISSCC. 1999 IEEE International, pp. 406–407. IEEE (1999)
282. Weigandt, T.C., Kim, B., Gray, P.R.: Analysis of timing jitter in CMOS ring oscillators. In: 1994 IEEE International Symposium on Circuits and Systems, 1994. ISCAS'94, vol. 4, pp. 27–30. IEEE (1994)
283. Van der Wel, A., Klumperink, E., Gierkink, S., Wassenaar, R., Wallinga, H.: Mosfet 1/f noise measurement under switched bias conditions. Electron Dev. Lett. IEEE **21**(1), 43–46 (2000)
284. Wens, M.: Monolithic inductive CMOS DC–DC converters: theoretical study & implementation (monolitische inductieve cmos DC–DC convertoren: Theoretische studie & implementatie). status: published (2010)
285. Wens, M., Cornelissens, K., Steyaert, M.: A fully-integrated 0.18 um CMOS DC–DC step-up converter, using a bondwire spiral inductor. In: ESSCIRC 2007, pp. 268–271 (2007). doi:10.1109/ESSCIRC.2007.4430295
286. Wentzloff, D., Chandrakasan, A.: Gaussian pulse generators for subbanded ultra-wideband transmitters. IEEE Trans. Microw. Theory Tech 54(4), 1647–1655 (2006). doi:10.1109/TMTT.2006.872053

287. Wikipedia: Cat's-whisker detector (2012). http://en.wikipedia.org/wiki/Cat's-whisker_detector
288. Wikipedia: Eniac (2012). http://en.wikipedia.org/wiki/ENIAC
289. Wikipedia: History of radar (2012). http://en.wikipedia.org/wiki/History_of_radar
290. Wikipedia: Leon theremin (2012). http://en.wikipedia.org/wiki/L%C3%A9on_Theremin
291. Wikipedia: Nikola tesla (2012). http://en.wikipedia.org/wiki/Nikola_Tesla
292. Wikipedia: Thing (listening device) (2012). http://en.wikipedia.org/wiki/Thing_(listening_device)
293. Wikipedia: Vacuum tube (2012). http://en.wikipedia.org/wiki/Vacuum_tube
294. Wikipedia: Amplitude modulation (2013). http://en.wikipedia.org/wiki/Amplitude_modulation
295. Wikipedia: Clock drift (2013). http://en.wikipedia.org/wiki/Clock_drift
296. Wikipedia: Edwin Howard Armstrong (2013). http://en.wikipedia.org/wiki/Edwin_Howard_Armstrong
297. Wikipedia: Gauss's law (2013). http://en.wikipedia.org/wiki/Gauss's_law
298. Wikipedia: Guglielmo marconi (2013). http://en.wikipedia.org/wiki/Guglielmo_Marconi
299. Wikipedia: History of the transistor (2013). http://en.wikipedia.org/wiki/History_of_the_transistor
300. Wikipedia: Invention of radio (2013). http://en.wikipedia.org/wiki/Invention_of_radio
301. Wikipedia: Invention of the Integrated Circuit (2013). http://en.wikipedia.org/wiki/Invention_of_the_integrated_circuit
302. Wikipedia: Magnetic detector (2013). http://en.wikipedia.org/wiki/Magnetic_detector
303. Wikipedia: Max wien (2013). http://en.wikipedia.org/wiki/Max_Wien
304. Wikipedia: Michael faraday (2013). http://en.wikipedia.org/wiki/Michael_Faraday
305. Wikipedia: Multivibrator (2013). http://en.wikipedia.org/wiki/Multivibrator
306. Wikipedia: Radio frequency identification (2013). http://en.wikipedia.org/wiki/Radio-frequency_identification
307. Wikipedia: Regenerative circuit (2013). http://en.wikipedia.org/wiki/Regenerative_circuit
308. Wikipedia: RMS titanic (2013). http://en.wikipedia.org/wiki/RMS_Titanic
309. Wikipedia: Spark-gap transmitter (2013). http://en.wikipedia.org/wiki/Spark-gap_transmitter
310. Wikipedia: Time (2013). http://en.wikipedia.org/wiki/Time
311. Wikipedia: Timeline of radio (2013). http://en.wikipedia.org/wiki/Timeline_of_radio
312. Wikipedia: Transistor radio (2013). http://en.wikipedia.org/wiki/Transistor_radio
313. Wikipedia: Wireless power (2013). http://en.wikipedia.org/wiki/Wireless_power
314. Wikipedia: Wireless sensor network (2013). http://en.wikipedia.org/wiki/Wireless_sensor_network
315. Wikipedia: James clerk maxwell (2014). http://en.wikipedia.org/wiki/James_Clerk_Maxwell
316. Williams, J.: Max wien, mr. hewlett, and a rainy sunday afternoon. In: Jim, W (ed.) Analog Circuit Design: Art, Science, and Personalities. Butterworth-Heinemann, Boston, pp. 43–55 (1991)
317. Williamson, T.: Oscillators for microcontrollers. Intel Application Note AP-155 (1983)
318. Wu, N.C., Nystrom, M., Lin, T.R., Yu, H.C.: Challenges to global rfid adoption. Technovation **26**(12), 1317–1323 (2006)
319. Wu, R., Chae, Y., Huijsing, J., Makinwa, K.A.A.: A 20-b 40-mv range read-out IC with 50-nv offset and 0.04 IEEE J. Solid State Circ. **47**(9), 2152–2163 (2012). doi:10.1109/JSSC.2012.2197929
320. Xu, Y.: Receiver architecture and methods for demodulating binary phase shift keying signals (2013). US Patent App. 14/034,426
321. Young, D., Keller, C., Bliss, D., Forsythe, K.: Ultra-wideband (UWB) transmitter location using time difference of arrival (TDOA) techniques. In: Conference Record of the Thirty-Seventh Asilomar Conference on Signals, Systems and Computers, 2004, vol. 2, pp. 1225–1229 (2003). doi:10.1109/ACSSC.2003.1292184

322. Zanchi, A., Bonfanti, A., Levantino, S., Samori, C.: General SSCR vs. cycle-to-cycle jitter relationship with application to the phase noise in PLL. In: 2001 Southwest Symposium on Mixed-Signal Design, 2001. SSMSD, pp. 32–37 (2001). doi:10.1109/SSMSD.2001.914933
323. van der Ziel, A.: On the noise spectra of semi-conductor noise and of flicker effect. Physica **16**(4), 359–372 (1950). doi:10.1016/0031-8914(50)90078-4.http://www.sciencedirect.com/science/article/pii/0031891450900784
324. van der Ziel, A.: Theory of shot noise in junction diodes and junction transistors. Proceedings of the IRE **43**(11), 1639–1646 (1955). doi:10.1109/JRPROC.1955.277990

Index

V. De Smedt et al., *Temperature- and Supply Voltage-Independent Time References for Wireless Sensor Networks*, Analog Circuits and Signal Processing 128,
DOI 10.1007/978-3-319-09003-0